



L-cysteine and N-acetyl-L-cysteine mediated synthesis of nanosilver-based sols and hydrogels with antibacterial and antibiofilm properties

Journal:	<i>Journal of Materials Chemistry B</i>
Manuscript ID	TB-ART-02-2023-000261.R1
Article Type:	Paper
Date Submitted by the Author:	n/a
Complete List of Authors:	Vishnevetskii, Dmitry; Tver State University, Department of Physical Chemistry Averkin, Dmitry; Tver State University, Physical Chemistry Efimov, Alexey; Moscow Institute of Physics and Technology National Research University, Lizunova, Anna; Moscow Institute of Physics and Technology National Research University Shamova, Olga; Research Institute of Experimental Medicine of North-Western Branch of Russian Academy of Medical Sciences Vladimirova, Elizaveta; Research Institute of Experimental Medicine of North-Western Branch of Russian Academy of Medical Sciences Sukhareva, Maria; Research Institute of Experimental Medicine of North-Western Branch of Russian Academy of Medical Sciences Mekhtiev, Arif; Institute of Biomedical Chemistry RAMS, Laboratory of the synthesis of the physiologically active compounds

Journal of Materials Chemistry B

Materials for biology and medicine

Guidelines for Reviewers

Thank you very much for agreeing to review this manuscript for [Journal of Materials Chemistry B](#).



Journal of Materials Chemistry B is a weekly journal in the materials field. The journal is interdisciplinary, publishing work of international significance on all aspects of materials chemistry related to applications in biology and medicine. Articles cover the fabrication, properties and applications of materials.

Journal of Materials Chemistry B's Impact Factor is **7.571** (2021 Journal Citation Reports®)

The following manuscript has been submitted for consideration as a
FULL PAPER

For acceptance, a Full paper must report primary research that demonstrates significant **novelty and advance**, either in the chemistry used to produce materials or in the properties/ applications of the materials produced. Work submitted that is outside of these criteria will not usually be considered for publication. The materials should also be related to the theme of biology and medicine.

When preparing your report, please:

- Focus on the **originality, importance, impact** and **reproducibility** of the science.
- Refer to the **journal scope and expectations**.
- **State clearly** whether you think the article should be accepted or rejected and give detailed comments (with references) both to help the Editor to make a decision on the paper and the authors to improve it.
- **Inform the Editor** if there is a conflict of interest, a significant part of the work you cannot review with confidence or if parts of the work have previously been published.
- **Provide your report rapidly** or inform the Editor if you are unable to do so.

Best regards,

Professor Jeroen Cornelissen

Editor-in-Chief

University of Twente, The Netherlands

Dr Michaela Mühlberg

Executive Editor

Royal Society of Chemistry

Contact us

Please visit our [reviewer hub](#) for further details of our processes, policies and reviewer responsibilities as well as guidance on how to review, or click the links below.



What to do
when you
review



Reviewer
responsibilities



Process &
policies

ARTICLE

L-cysteine and N-acetyl-L-cysteine mediated synthesis of nanosilver-based sols and hydrogels with antibacterial and antibiofilm properties[†]

Received 00th January 20xx,
Accepted 00th January 20xx

DOI: 10.1039/x0xx00000x

Dmitry V. Vishnevetskii,^{a*} Dmitry V. Averkin,^{a,b} Alexey A. Efimov,^c Anna A. Lizunova,^c Olga V. Shamova,^d Elizaveta V. Vladimirova,^d Maria S. Sukhareva^d and Arif R. Mekhtiev^e

The problem of the synthesis of a new generation of medicines aimed at combating bacteria and biofilms caused various infections is a great urgency. There is a gradual departure from conventional techniques of treatment with the use of antibiotics, and consequently, the search for new methods and approaches for obtaining and rational use of available antibacterial drugs to which microorganisms do not acquire resistance. Although silver nanoparticles (AgNPs) and silver nanoclusters (AgNCs) have exhibited certain effectiveness against multidrug-resistant bacteria and biofilms, there are too few simple, cheap and easy-to-scale methods for AgNPs and AgNCs obtaining with well-desired characteristics. In this work, we have carried out the one-pot synthesis of sols and gels containing AgNPs and AgNCs using the only L-cysteine (CYS) or N-acetyl-L-cysteine (NAC) as bioreducing/capping/gel-forming agents and different silver salts – nitrate, nitrite and acetate. HRTEM, SAED, EDX mapping, AFM, SEM, EDX, ICP-MS and FTIR analysis confirmed the formation of spherical/elliptical CYS-AgNPs and NAC-AgNCs particles consisting of AgNPs or AgNCs “core” and CYS/Ag⁺ or NAC/Ag⁺ complexes “shell” with mean average diameter of 10 and 5 nm respectively. UV-Vis spectroscopy fixed localized surface plasmon resonance (LSPR) at 390–420 nm for CYS-AgNPs systems and LSPR absence for NAC-AgNCs ones. DLS and nanoparticle tracking analysis (NTA) data indicated that mean average diameter of particles is about 80 nm for CYS-AgNPs systems and 20 nm for NAC-AgNCs ones. Zeta potential measurements showed particles possess the positive and negative charge values for CYS-AgNPs and NAC-AgNCs systems respectively. The prepared materials demonstrated the high antibacterial activity against the most common types of bacteria at MIC range of 10–100 μM, wherein, the effect of NAC-AgNCs systems in 2 times stronger than CYS-AgNPs ones. The both systems are non-toxic/low-toxic at 300 μM for the normal human cells: erythrocytes, fibroblasts and macrophages. Sols and hydrogels in concentration range of 20–40 μM showed the complete inhibition of formation of biofilms *Acinetobacter baumannii* and *Pseudomonas aeruginosa* belonging to ESKAPE pathogenes group and representing the most serious problem in practical medicine. NAC-AgNCs systems were the most active. The simple strategy of the preparation of AgNPs/AgNCs-based sols and gels along with their pronounced antibacterial and antibiofilm activity could open the perspectives for it applications in medicine.

Introduction

The multidrug-resistant bacteria and especially biofilms are cause of the various infections: more than 65% of nosocomial, 80% of chronic and 60% of all human bacterial ones.¹ Biofilm-associated diseases increase the human morbidity and mortality rates and economic burdens because of high healthcare costs and prolonged patient stays.² Although antibiotics were the main antibacterial drugs in the

past century, their frequent and excessive use lead to the extensive multidrug resistance.³ The problem is complicated by the fact that biofilms are inherently insensitive to antibiotics and are upwards of 1000-fold more resistant to them than planktonic bacteria.⁴ Thus, the search and development of an effective and safe medicines against bacteria and biofilms is a great challenge. There have been extensive studies related to the creation of new materials for the elimination of biofilms using small molecule agents,⁵ carbon nanomaterials⁶, macromolecular species⁷ and inorganic nanoparticles.⁸ The latter have a significant place in the field of biomedical applications due to a unique range of properties: antibacterial, anticancer, magnetic, optoelectrical, biosensing, bio-imaging and etc.^{9,10} Among of them silver nanoparticles (AgNPs) are one of the promising candidates in the therapy of the different infectious diseases and medical devices owing to their broad-spectrum antibacterial activity and little drug resistance.^{11–15} It has been shown that properties of AgNPs – cytotoxicity and bioactivity directly depend on their characteristics: size, distribution, morphological shape and surface charge.¹⁶ Furthermore, AgNPs can

^aDepartment of Physical Chemistry, Tver State University, Tver 170100, Russia.

E-mail: rickashet@yandex.ru

^bRussian metrological institute of technical physics and radio engineering, Moscow 141570, Russia

^cMoscow Institute of Physics and Technology, National Research University, Dolgoprudny 141701, Russia

^dWorld-Class Research Center “Center for Personalized Medicine”, Institute of Experimental Medicine, St. Petersburg 197376, Russia

^eInstitute of Biomedical Chemistry, Moscow 119121, Russia

[†]This work is dedicated to prof. Maxim M. Ovchinnikov and Nadezhda A. Vishnevetskaya.

^{††}Electronic Supplementary Information (ESI) available: UV, HRTEM, SAED, EDX mapping, SEM, EDX, AFM, ICP-MS, DLS, NTA, Zeta-potential measurements, FTIR, Antibacterial assay, Hemolysis assay, MTT-test See DOI: 10.1039/x0xx00000x

easily agglomerate and oxidize that leads to suppression of their antibacterial and antibiofilm capacities.¹⁷ Hence, the practical applications of AgNPs need to use the biocompatible and either non-toxic or low-toxicity synthetic protocols along with remaining of the high activity of obtained AgNPs.

We have lately mentioned about various biological approaches which use “green” nanotechnologies for AgNPs synthesis, considered their disadvantages and come to conclusion that one of the best ways is to use the low molecular weight bio-reducing agent without any other related components in its initial solution, for instance, amino acids.¹⁸⁻²¹ We have shown that L-cysteine (CYS) can simultaneously act as a reducing, capping and gel-forming agent at the simplest mixing of its aqueous solution with silver salts at ambient conditions.²¹⁻²⁵ As a result of the research, we have previously found out that the surface state and the size of obtained nanoparticles directly determine the ability of the system to form a gel, as well as the properties of the final material: anticancer, catalytic, electrochemical, film-forming.

The number of articles which is devoted to the production and application of silver nanoparticles grow every year, while recently there has been more and more information about the synthesis and various properties of silver nanoclusters (AgNCs).^{26,27} It is well known that some of metal nanoparticles possess the characteristic absorption band in the UV spectrum, called localized surface plasmon resonance (LSPR), occurring due to a coherent and collective oscillation of the electrons on the nanoparticle surface when interacting with light of a wavelength much bigger than the particle size.²⁸ The picture absolutely changes in the case of AgNCs: no LSPR observed since all conducting electrons are now quantized, losing all metallic properties because of quite small sizes of particles.²⁹

AgNCs have demonstrated some superior properties over AgNPs. They possess stronger bioactive effect (antibacterial, anticancer and etc.) compared to AgNPs due to their less size.^{30,31} This fact, besides, determines less toxicity of AgNCs even in the *in vivo* experiments. For instance, they penetrate through the kidney barrier much better opposed to AgNPs and it allows them to be efficiently cleared from the body without causing serious damage.³²

There are several strategies for AgNCs synthesis such as direct reduction,^{33,34} chemical etching^{35,36} and ligand exchange.^{37,38} Organic ligands such as thiolates, phosphines, and alkynyls are usually used to cap on the surface in order to prevent aggregation and to facilitate the isolation of target AgNCs.³⁹⁻⁴¹ However, all of these approaches are quite expensive and (or) toxic reagents are used, consequently it can't be easy scalable, safe for humans and the environment.

In the present article, we delved into the study of the self-assembly process with partaking of sulfur-containing amino acids and silver salts. To do this, firstly, we used additional methods for analyzing the structure of obtained nanoparticles, and, secondly, for the first time, we investigated in detail the behavior of systems obtained at mixing of N-acetyl-L-cysteine (NAC) aqueous solutions with silver salts. NAC is well-known available mucolytic, expectorant, antioxidant agent. An unexpected result was that the replacement of CYS with NAC lead to the formation of non-crystalline silver phase – silver clusters. This system turned out to be twice more active in planktonic bacteria suppression and more importantly their biofilms in *in vitro* experiments. CYS-AgNPs and NAC-AgNCs were non-toxic or

have the low toxicity to the normal human cells in culture. Thus, the novel “green” chemistry approach could open perspectives for the silver-related materials production with the enhanced desired properties.

Experimental

Chemicals

L-cysteine (>99 %) and N-acetyl-L-cysteine (>98 %) were obtained from Acros. Silver nitrite (>99 %), silver nitrate (>99 %) and silver acetate (>99 %) were purchased from Lancaster. All chemicals were used as received. All solutions were prepared on de-ionized water after its filtration on 0.45 μm filters.

General procedure for the preparation of CYS-AgNPs and NAC-AgNCs systems

The solutions (2 mL) were prepared by the following scheme (as an example): the empty vessel 0.8 mL of the de-ionized water was filled, then 0,6 mL of L-cysteine or N-acetyl-L-cysteine (0.01 M) was added, finally 0.6 mL of silver salt (0.01 M) was added (Table 1). 0.15 mL of Na₂SO₄ (0,01 M) as a gelation agent was added in SS-1 and SS-3 samples. The resulting mixtures were stirred at room temperature (25°C) for 1 minute and solutions were stayed in dark place for 3 hours. As a result, from uncolored to yellow or brown transparent solutions or hydrogels were obtained.

Table 1 The synthetic protocol for CYS-AgNPs and NAC-AgNCs systems.

Abbr. of sample	Sample	Water, mL	Amino acid, mL	Silver salt, mL
SS-1	CYS-AgNO ₃	0.65	0.6	0.75
SS-2	CYS-AgNO ₃ -SO ₄ ²⁻	0.65	0.6	0.75
SS-3	CYS-AgOOCCH ₃	0.65	0.6	0.75
SS-4	CYS-AgOOCCH ₃ -SO ₄ ²⁻	0.65	0.6	0.75
SS-5	CYS-AgNO ₂	0.8	0.6	0.6
SS-6	CYS-AgNO ₂	0.65	0.6	0.75
SS-7	NAC-AgOOCCH ₃	0.8	0.6	0.6
SS-8	NAC-AgOOCCH ₃	0.65	0.6	0.75
SS-9	NAC-AgNO ₂	0.8	0.6	0.6
SS-10	NAC-AgNO ₂	0.65	0.6	0.75

HRTEM, SAED and EDX mapping analysis

The microstructure and elemental mapping analysis of the samples were analyzed using a transmission electron microscope JEM-2100 (JEOL Ltd.), equipped with the energy dispersive X-ray spectrometer X-MAXN OXFORD instruments, with an accelerating voltage of up to 200 kV. Samples were placed on a standard copper grid with a 100 nm thick Formvar (polyvinylformal) polymer support, dried, and placed in the microscope.

AFM analysis

The surface topography of the samples was investigated by using a

scanning probe microscope Solver Next (NT-MDT) in the semi-contact mode.

SEM and EDX

The microstructure and chemical composition of the samples were also studied using a raster JEOL 6610 LV electron microscope (JEOL Ltd.) with x-ray system energy dispersive microanalysis Oxford INCA Energy 350. in a high vacuum mode with accelerating voltage of 15 kV. Samples preparation was consisted of its spraying on the surface of a thin conductive layer of platinum and drying in vacuum (10^{-4} Pa).

UV-Vis spectroscopy

Electronic spectra of the samples were recorded on the UV spectrophotometer Evolution Array (Thermo Scientific) in a quartz cell with a 1 mm path length.

DLS and zeta potential measurements

Measurement of intensity of light scattering in the studied samples was carried out using analyzer Zetasizer Nano ZS (Malvern) with He-Ne laser (633 nm), power of 4 mW. The solutions were filled in polystyrene cuvette without any other manipulations. For the correct analysis of the particle sizes and zeta-potential in gel state, the samples were mechanically destroyed and diluted two, four and eight times. All measurements were carried out at 25°C in the backscattering configuration (173°), providing the highest sensitivity of the device. Mathematical processing of the results of the obtained cross-correlation functions of the diffuse light intensity fluctuations g_2 was carried out in the program Zetasizer Software, where the solution of the obtained equation of the g_2 dependence on the diffusion coefficient was performed by the cumulant method. The result of the solution was the function $z(D)$. The hydrodynamic radii of the scattering particles were calculated from the diffusion coefficients by the Stokes-Einstein formula: $D = kT/6\pi\eta R$, where D is the diffusion coefficient, k is the Boltzmann constant, T is the absolute temperature, η is the viscosity of the medium, R is the radius of the scattering particles. Measurement of the electrophoretic mobility of aggregates in the samples was carried out in U-shaped capillary cuvettes. Zeta potential distributions were calculated using the Henry equation: $UE = 2\epsilon z f(Ka)/3Z$, where UE – electrophoretic mobility, z – zeta potential, ϵ – dielectric constant, Z – viscosity, and $f(Ka)$ – Henry's function, $f(Ka) = 1.5$ for aqueous media.

NTA

The measurements were made with a NanoSight NS300 (Malvern) equipped with a scientific CMOS camera, a 20x objective lens, a blue laser module (405nm, LM12 version C) and NTA software version 3.1. A 1-mL disposable syringe was used to inject the samples into the instrument chamber. For the correct analysis of the particle sizes in gel state, the samples were mechanically destroyed and diluted two, four and eight times. The video data were collected for 30 seconds, repeated three times for each sample. The detection threshold of the NTA software was set to 5 and the maximum jump distance and the minimum track segment length were both set to auto.

ICP-MS analysis

The "PlasmaQuant MS" (Analytik Jena GmbH) mass spectrometer with inductive coupled plasma was used. ICP-MS is equipped with

Scott spray chamber with double passage. The mass spectrometer used argon gas (chemical purity of 99.993%). The sputtering efficiency was determined using a colloidal solution of β -cyclodextrin-stabilized Ag/CDx/W silver nanoparticles with a nominal particle size of 12 nm. The controlled isotope was ^{107}Ag . To quantify the ^{107}Ag intensity in time resolved analysis mode to take ICP-MS data on reconstituted Ag/CDx/W silver nanoparticles diluted to Ag mass fractions from 500 $\mu\text{g/L}$ to 0.25 $\mu\text{g/L}$. Solution of diluted nanoparticles was introduced via peristaltic pump into low-flow (0.7 mL/min) concentric nebulizer and impact bead spray chamber cooled to 2°C. The delay time was set at 3 ms with typical data collection time of 60 s for each measurement.

pH measurements

The pH of the solutions was measured using a Seven Multi S70 (Mettler Toledo) pH meter.

FTIR spectroscopy

FTIR spectra of the samples were recorded on a Vertex 70 spectrometer (Bruker) in the range of 7000–400 cm^{-1} at a resolution of 4 cm^{-1} . The number of scans was 32. The studied samples (solutions and hydrogels) were preliminarily frozen in a liquid nitrogen; the obtained uncolored, yellowish or brown precipitates were carefully washed with de-ionized water and vacuum dried at 25°C. 22 mg of the precipitate was mixed with 700 mg of potassium bromide and pressed into a pellet.

MTT test Wi-38 cells

Wi-38 human normal embryonic lung cells obtained from the American Tissues and Cells Collection (ATCC) were cultivated in 96-well plates at 37°C in atmosphere of 5% CO_2 in a DMEM medium with the addition of L-glutamine (2 mM), antibiotics (100 units per mL of penicillin and 100 $\mu\text{g/mL}$ of streptomycin), and 10% of FBS. The cells were incubated in a serum medium with the tested compounds at various concentrations for 48 h. PBS (10 μL) containing MTT (5 mg/mL) was added to each well, and the cells were incubated at 37°C for 4 h. The culture medium was removed, DMSO (100 μL) was added to each well, a plate was vortex for 20 minutes, and then the optical absorbance in each well was measured at 570 nm in a Multiskan Spectrum Microplate Reader instrument (Thermo Scientific, United States). The MTT test readings were averaged for three independent determinations. Readings of MTT test in the absence of the tested compounds were taken as 100%.

MTT test macrophage cells

The human monocytic leukemia cell line - THP-1 - obtained from ATCC (American Type Culture Collection, Manassas, Virginia) were cultured in RPMI 1640 medium containing 10% fetal bovine serum (FBS), 2 mM L-glutamine, 100 U/mL penicillin, and 100 $\mu\text{g/mL}$ streptomycin (growth medium), at 37°C in an atmosphere containing 5% CO_2 . The cells ($5 \times 10^5/\text{mL}$) were washed and suspended in the same medium, contained phorbol ester (PMA-phorbol 12-myricate-13 acetate (Sigma)) to a final concentration of 100 ng/mL to initiate their transformation into macrophages. The cells ($5 \times 10^3/\text{well}$) were transferred to 96-well plates and incubated for 48 h at 37 °C and 5% CO_2 . Then the cells were incubated in a serum medium with tested compounds at various concentrations for 48 h. PBS (10 μL) containing MTT (5 mg/mL) was added to each well, and the cells were incubated

at 37°C for 4 h. The culture medium was removed, DMSO (100 µL) was added to each well, a plate was vortex for 20 minutes, and then the optical absorbance in each well was measured at 570 nm in a Multiskan Spectrum Microplate Reader instrument (Thermo Scientific, United States). The MTT test readings were averaged for three independent determinations. Readings of MTT test in the absence of the tested compounds were taken as 100%.

Hemolysis assay

Hemolytic activity of samples toward human erythrocytes was determined using a standard protocol (Tossi et al., 1997). Peripheral blood of healthy volunteers was collected into EDTA-coated vacutainer tubes and then repeatedly washed with phosphate-buffered saline (PBS), precooled to 4°C, to remove any trace of plasma components and of anticoagulant. The washing cycle included centrifuging the samples at 300 g at 4°C for 10 min, removing the supernatant and resuspending the cells in a fresh aliquot of PBS. After the third round, 280 mL of cellular precipitate were resuspended with PBS up to 10 mL to obtain a suspension of stock red blood. 90 µL of this stock were mixed with 10 µL of the tested systems, also diluted in PBS to various concentrations; the end concentration of erythrocytes was 2.5% v/v. Mixtures were incubated for 30 min at 37°C and then centrifuged for 3 min at 10,000 g. Hemoglobin release from the lysed erythrocytes was spectrophotometrically measured in the supernatants at 540 nm, using a SpectraMax 250 Spectrophotometer (Molecular Devices, USA). The percentage of hemolysis in test samples was calculated by comparison to a positive control for total hemolysis (100% lysis) where 10 µL of 1% v/v Triton X-100 was used instead of the investigated systems, and with a negative control (0% lysis) where only PBS was added to erythrocytes, according to the following formula:

$$\text{Hemolysis(\%)} = \frac{(OD_{\text{sample}} - OD_{0\% \text{ lysis}})}{(OD_{100\% \text{ lysis}} - OD_{0\% \text{ lysis}})} \times 100\%$$

where OD_{sample} , $OD_{0\% \text{ lysis}}$, and $OD_{100\% \text{ lysis}}$ are respectively the optical density values at 540 nm for the test sample and the negative and positive controls. Experiments were repeated three times and in each case in triplicate (samples and controls). Tests were carried out in accordance with the Declaration of Helsinki, written informed consent was given by all donors beforehand.

Antibacterial Assays

Bacterial strains used were as follows: laboratory strains of *Staphylococcus aureus* ATCC 25923 were kindly provided by Dr. Elena Ermolenko (Institute of Experimental Medicine, St-Petersburg, Russia); drug-resistant bacterial strains *Acinetobacter baumannii* 7226/16 (resistant to imipenem, gentamicin, tobramycin, ciprofloxacin, trimethoprim/sulfamethoxazole), *Pseudomonas aeruginosa* 522/17 MDR (resistant to meropenem, ceftazidime, cefixime, amikacin, gentamicin, netilmicin, ciprofloxacin, colistin), from the urine of patients were generously supplied by Dr. A. Afinogenova from the Research Institute of Epidemiology and Microbiology named after L. Pasteur, Saint Petersburg, Russia; clinical isolate of *Staphylococcus intermedius* (resistant to ciprofloxacin, cefuroxime, clindamycin, erythromycin, rifampicin, gentamicin, benzylpenicillin, and oxacillin) obtained from an infected

wound caused by a dog bite was provided by colleagues from the S.M. Kirov Military Medical Academy (Saint Petersburg, Russia). Initial susceptibility testing was performed by their colleagues from said institutions.

Broth Microdilution Assay

The minimal inhibitory concentrations (MIC) of CYS-AgNPs and NAC-AgNCs systems were determined using microdilution assay in Müller–Hinton (MH) broth in general accordance with the guidelines of the European Committee for Antimicrobial Susceptibility Testing. The procedure is described in (Zharkova et al., 2021). Briefly, two-fold serial dilutions of investigated samples starting with 2 × stock concentration were prepared in sterile phosphate-buffered saline (PBS). Thus, final solutions contained 50% of PBS diluted tested samples and 50% of MH broth with bacteria. Bacteria for testing were grown overnight, then transferred into a fresh portion of 2.1% MH medium and additionally incubated for 2–3 h to obtain bacterial culture in its mid-logarithmic growth phase, which was diluted down to the final concentration of 1×10^6 CFU/mL.

Biofilm Formation Assessment by the Crystal Violet Assay

Quantification of the biofilms forming in the presence of various concentrations of tested systems was performed using the crystal violet assay according to general guidelines (Merritt et al., 2006). Tests were performed in polystyrene 96-well plates with U-shaped bottom. CYS-AgNPs and NAC-AgNCs systems were serially diluted in a bacterial growth medium (MH for *A. baumannii* or TSB for *P. aeruginosa*) in a volume of 50 µL per well. Overnight cultures of tested bacteria in a stationary phase of growth were 50 times diluted and introduced into the experimental wells at the same volume of 50 µL. Samples were incubated for 24 h at 37°C. The content of the wells was then shaken out, the plates were gently washed from unattached planktonic bacteria in still water (poured into a large enough vessel); bacterial cells and matrix components adhered to the walls of the wells were stained with a 0.1% aqueous solution of crystal violet dye: 125 µL of dye solution was put into each well and incubated at room temperature for 10 min. After staining dye solution was removed, the plates were washed with clean water and allowed to air-dry. Finally, the bound dye was redissolved by adding 200 µL of 30% acetic acid into each well, incubating it for 15 min at room temperature, and then thoroughly mixing the content of the wells by pipetting. One hundred and twenty five microliters of crystal violet extract from each well were transferred into a flat-bottomed microtiter plate, and the optical density was measured at a wavelength of 560–595 nm (depending on the maximum of absorption in a particular experiment). Experimental samples were made in quadruplicates, and there were 8–9 repeats of control samples without CYS-AgNPs and NAC-AgNCs systems in each test. Presented results are medians calculated based on 3 independent experiments.

Results and discussion

Synthesis of CYS-AgNPs and NAC-AgNCs systems

In the present study we have synthesized a set of systems by varying

the chemical nature of the silver salt and amino acid, their concentration and ratio based on the results of our preliminary research.²¹ The main idea was to show the similarities and differences of NAC and CYS reaction with various silver salts. At mixing of aqueous solution of CYS and silver salt, regardless of its chemical nature, from yellow-green to brown-colored solutions or thixotropic gels are obtained in the concentration range of the dispersed phase of 1-20 mM (Fig. 1a, Fig. S1,1). In the case of silver nitrate and acetate, the gel formation requires the addition of low molecular weight anions (Cl^- , SO_4^{2-}), whereas for silver nitrite the gel forms without any other components. Some rheological properties and aspects of the gelation mechanism of these systems have been lately studied.²¹ At a fixed concentration of the amino acid, the higher the silver content in the system, the richer the color of the samples. And we have expected the same behavior for NAC. However, one can see that in this case the uncolored solutions are obtained with AgNO_2 and AgOOCCH_3 (Fig. 1b, Fig. S1,2). The interaction of NAC with AgNO_3 gives the white precipitates which is probably dealt with the silver mercaptide formation. The homogeneous samples were SS-1 – SS-10 (Table 1), that's why further we studied mainly these systems. It should be noted that during more 6 months the samples for both – CYS and NAC systems remain stable – no opalescence, precipitation or color changing was fixed. And it was controlled by UV-Vis analysis, DLS and zeta potential measurements. Thus, it is even visually obvious that the behavior of these systems is very different from each other. Therefore, we used an integrated approach to study this phenomenon.

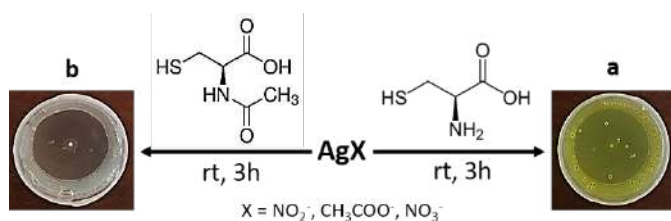


Fig. 1 Scheme of a - CYS-AgNPs and b - NAC-AgNCs systems preparation. $C(\text{CYS}) = C(\text{NAC}) = 3 \text{ mM}$, $C(\text{AgX}) = 3.75 \text{ mM}$ in the final solution.

Characterization of CYS-AgNPs and NAC-AgNCs systems

Since the systems have or haven't the color, one can expect that it must or mustn't absorb quanta of light at a certain wavelength. The principal difference of UV spectra of CYS-AgX and NAC-AgX systems (Fig. 2) is the absence of the absorption band at 390-410 nm for latter one which is responsible for localized surface plasmon resonance (LSPR) of silver nanoparticles.²¹ Widened bands at 280 and 310 nm are attributed to the ligand-to-metal charge-transfer transition (LMCT) and argentophilic interactions in CYS/Ag⁺ complexes respectively.²¹ The growth of the LSPR band and its shift to the region of large wavelengths occurs at increase of the silver content in CYS-AgX systems. Meanwhile, no changes observe for NAC-AgX ones in this region (Fig. 2,a,c). The wide band at 280-310 rises in both systems. The absorption of LSPR band grows at increasing the concentration of the dispersed phase only for CYS-AgX systems and no changes take place for NAC-AgX ones (Fig. 2b,d). It should be noted that at the concentration of the dispersed phase < 1mM LSPR vanished for both systems and samples are uncolored (Fig. S2).

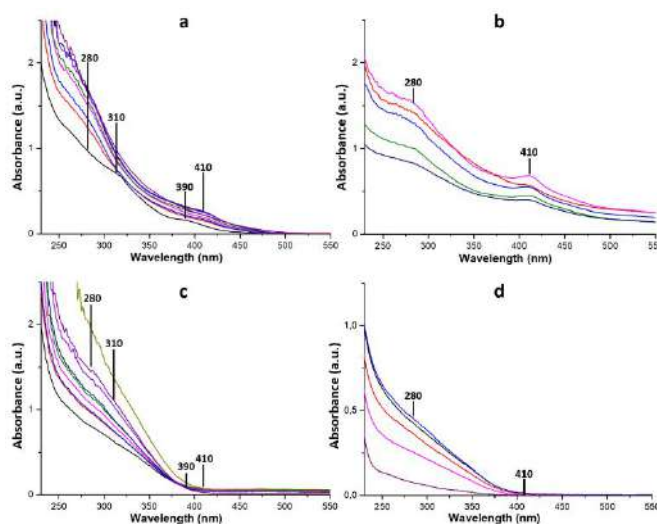


Fig. 2 UV-spectra of a,b - CYS-AgNPs and c,d - NAC-AgNCs systems. a,c - $C(\text{CYS}) = C(\text{NAC}) = 3 \text{ mM}$, $C(\text{AgX}) = 1.5 - 6 \text{ mM}$; b,d - $C(\text{CYS}) = C(\text{NAC}) = 10 \text{ mM}$, $C(\text{AgX}) = 5 - 20 \text{ mM}$.

At higher than 20 mM dispersed phase concentration the white or brown⁴² precipitates are obtained. So, it can be assumed based on the mentioned above data and lately obtained⁴² that the LSPR band is responsible for the color of the samples.

Results obtained by transmission electron microscopy are demonstrated on the Fig. 3 (Fig. S3, S4, S5). The morphology of all systems is the network of filament-like structures constructed from spherical/elliptical nanoparticles of mean average diameter of 5-10 nm. The densest network is observed for CYS-AgNO₂ system (Fig. 3A) because of it forms the gel without any additional components unlike other systems. CYS-AgNO₃ and CYS-AgOOCCH₃ systems can form a gel at initiation by the sulphate-anion (Fig. S5). SAED analysis fixes diffraction rings and reflexes corresponding to 111, 200, 220 and 311 planes of the face-centered cubic lattice of the crystalline phase of silver nanoparticles in the case of CYS-AgX systems and no rings/reflexes for NAC-AgX ones (Fig. 3B, S4). One can also be noted that the increase of the silver salt concentration in CYS-AgX samples leads to rising of the number AgNPs, their sizes and growing of diffraction intensity (Fig. S3). HRTEM shows silver atoms in CYS-AgX systems are close-packed and clear ordered, the interplane distance of 2,33 Å is consistent with the 111 plane of AgNPs (Fig. 3,C,D, S3, S4). This is not taken place for NAC-AgX systems. EDX mapping analysis confirms these data, herewith sulfur atoms are localized on the surface of silver atoms in CYS-AgX systems and both on silver atoms and between them in NAC-AgX ones (Fig. 3,E, S3, S4). These results are in a good agreement with UV analysis data. AFM, SEM, EDX and ICP-MS verify the results of TEM concerning the composition, the character of particle distribution, and their sizes in samples (Fig. S6).

Hydrodynamic and electrokinetic parameters of systems are presented on the Fig. 4 (Fig. S7). Nanoparticles in both systems have the unimodal size distribution that confirms via NTA and DLS. And these methods conform each other. The polydispersity coefficient of particles decreases at moving from CYS to NAC systems. The surface of particles is positively charged in CYS-AgX systems and negatively in NAC-AgX. This is due to the fact that the amino-group is blocked in NAC, thus only the carboxyl group can protonate/deprotonate in this

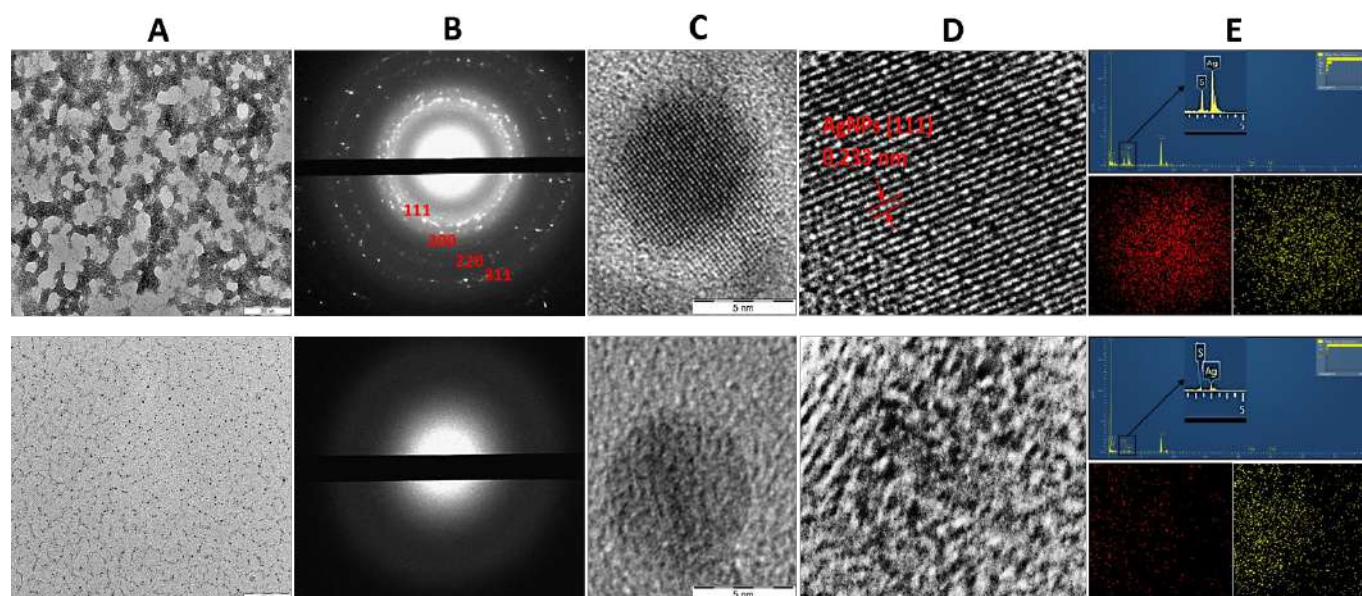


Fig. 3 A – TEM, B – SAED, C, D – HRTEM, E – EDX mapping analysis (red and yellow colour – silver and sulphur atoms respectively) images for CYS-AgNO₂ (Top) and NAC-AgNO₂ (Bottom) systems.

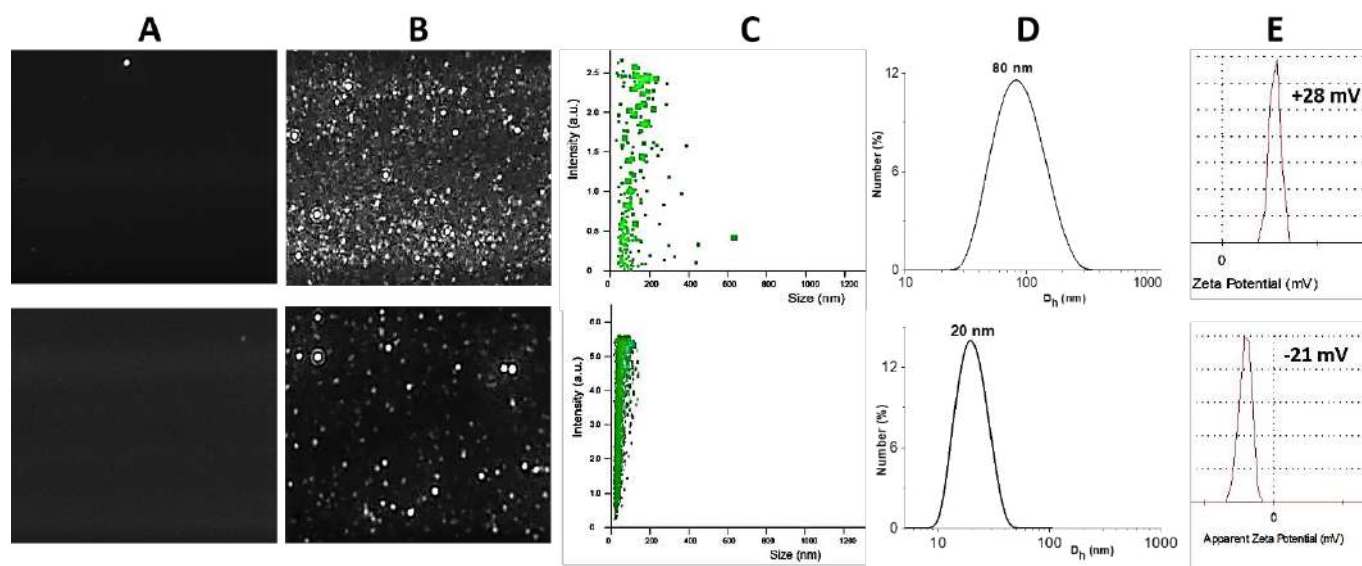


Fig. 4 A, B – NTA instant photos of pure water and SS systems respectively, C – particles size distribution by NTA, D - particles size distribution by DLS, E – zeta-potential measurements for CYS-AgNO₂ (Top) and NAC-AgNO₂ (Bottom) systems.

case. pH of resulted samples is 2.60 – 4.10 in dependence of chemical nature of amino acid and silver salt,²¹ herewith, amino-groups are fully protonated and carboxyl ones partly. pH of initial solutions of amino acids is 5.20-5.40. Thus, the addition of the silver salt to amino acid solution leads to the medium acidification.

FTIR-spectra of initial amino acids change after adding of silver salts (Fig. S8). The same peculiarity for both CYS-AgX and NAC-AgX systems is the disappearance of the $\nu(\text{SH})$ at 2552 cm^{-1} that points to interaction of silver ions with thiol-groups of amino acids.

Summing up of the current data one can propose the following mechanism of the self-assembly (Fig. 5): silver ions interact primarily

with thiol-groups of amino acids that is in a good agreement with Pearson's HSAB (hard and soft (Lewis) acids and bases) theory, meanwhile two parallel reactions may occur – the formation of so-called CYS(NAC)/Ag⁺ complexes and the reduction of Ag⁺ to zero valent state. The presence of Ag⁰ in the systems is beyond doubt. It is known, CYS possesses a middle reduction properties^{43,44} and 15-times higher reduction ability to silver ions compared to hydrazine hydrate.⁴⁵ Herewith, L-cysteine is a stronger reducing agent than N-acetyl-L-cysteine.⁴⁶ That's why crystalline phase of AgNPs occurs only in the presence of CYS, whereas the non-crystalline phase of silver clusters takes place for NAC. The other and more difficult question is

dealt with peculiarities of CYS(NAC)/Ag⁺ complexes formation and their structure. According to our previous,^{21,22,25} present data and literature,⁴⁷⁻⁵⁰ we can propose that CYS/Ag⁺ and NAC/Ag⁺ complexes have the similar structure (Fig. 5, blue chains). The interaction of stabilized AgNPs or AgNCs with these complexes, seemed, proceeds via formation of hydrogen bonds between charged amino- and carboxyl groups in the case of CYS systems (Fig. 5, a) or partly protonated carboxyl groups for NAC ones (Fig. 5, b) and it leads to the formation of final particles. Furthermore, complexes interact with each other via hydrogen bonding and form sandwich-like shell. Thus, particles are constructed from the core of AgNPs or AgNCs and shell of CYS/Ag⁺ or NAC/Ag⁺ complexes. Amino- and carboxyl groups are located on the surface of particles and responsible for their solubility and colloidal stability of systems. Meanwhile, the smaller hydrodynamic parameters of particles in NAC systems are due to the fact that most of NAC/Ag⁺ complexes interact with silver clusters and form the particle core, these data are consistent with HRTEM and EDX mapping analysis. In confirmation of such structure of particles for NAC systems is the fact that LSPR occurs also on the surface of small individual silver clusters⁵¹⁻⁵³ but in our case AgNCs link into a single particle and plasmons are seemed quench each other inside of this particle. So, one can expect that the difference in the structural parameters of particles in CYS and NAC systems must significantly affect to it final bioactive properties.

Bioactive properties of CYS-AgNPs and NAC-AgNCs systems

In accordance with the literature, there are a literally several articles related to methods of the synthesis of silver nanoparticles and silver clusters using sulfur-containing amino acids, as well as the study of bioactive properties of obtained compositions (Table 2). All of these synthetic techniques use toxic reducing agents⁵⁴⁻⁵⁸ or additional external exposures,⁵⁹ the antibacterial effect has either not been studied at all, or it is 1-2 orders of magnitude lower compared to studied samples in the present work. Furthermore, investigated systems are not inferior in antibacterial activity to other known silver-based systems.⁶⁰ Concerning systems under study, one can see their activity to gram-negative bacteria is more pronounced than on gram-positive ones (Table 2, Table S1, Fig. S9,1,2). This phenomenon can be explained by existing difference in the thickness of the cell wall in gram-positive (30 nm) and gram-negative (3-4 nm) bacteria.⁶¹ MIC of CYS systems reduced at moving from SS-1 to SS-6 system and further to NAC systems (SS-7 - SS-10) for gram positive bacteria, but its values were practically the same for gram negative ones. The total bioactive effect against all bacteria is twice as high for systems based on NAC. The solutions of initial amino acids showed no activity at concentrations 2 orders of magnitude higher than MIC of SS-1 - SS-10.

It is known, silver ions are more harmful to the various normal human cells than silver nanoparticles.⁶² The other problem is a high reactivity of Ag⁺ to different anionic compounds of blood plasma that leads to precipitation. Reducing the toxicity of silver-based systems is a key task in the development of new drugs for antibacterial

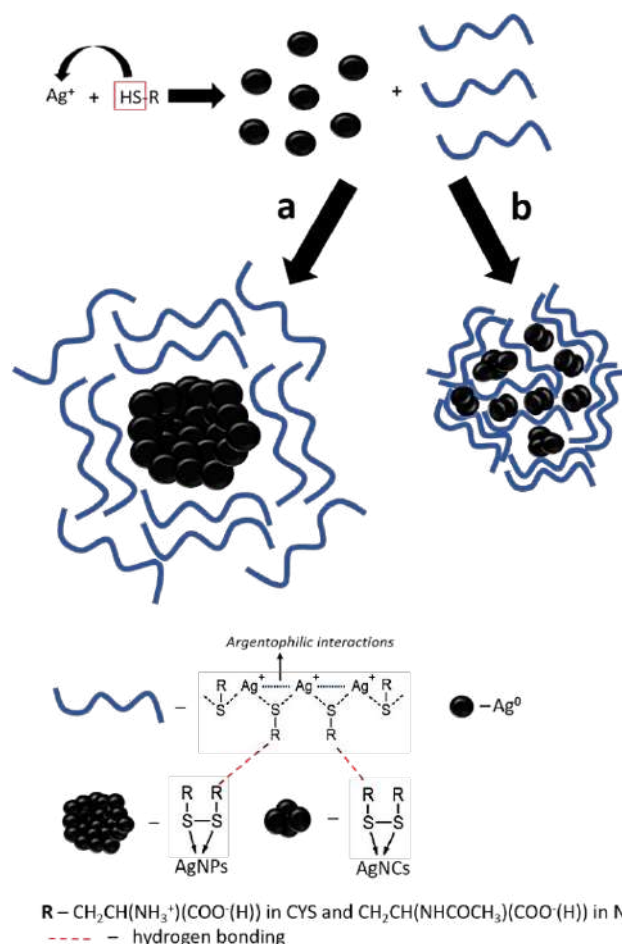


Fig. 5 The proposed mechanism of core-shell like structure particles formation.

Table 2 The synthetic protocol and antibacterial activity (MIC) of SS-1 – SS-10 samples and other related systems to planktonic bacteria.

Sample	Reducing/stabilizing agent	MIC, μM gram-positive/negative bacteria	Ref.
SS-1	CYS/CYS	1500/23,45	Our work
SS-2	CYS/CYS	750/23,45	Our work
SS-3	CYS/CYS	562,5/23,45	Our work
SS-4	CYS/CYS	234,38/23,45	Our work
SS-5	CYS/CYS	281,25/93,75	Our work
SS-6	CYS/CYS	140,63/46,9	Our work
SS-7	NAC/NAC	46,9/11,7	Our work
SS-8	NAC/NAC	93,75/23,45	Our work
SS-9	NAC/NAC	93,75/23,45	Our work
SS-10	NAC/NAC	93,75/23,45	Our work
Ag _n (NALC) _m	NaBH ₄ /NAC	3700/6400	54
nano-Ag	TBAB/CYS	-/93	55
CYS capped AgNPs	NaBH ₄ /CYS	-/-	56
L-CYS-AgNPs	NaBH ₄ /CYS	-/-	57
CYS capped AgNPs	NaBH ₄ /CYS	-/-	58
CYS-AgNPs	UV/CYS	-/-	59

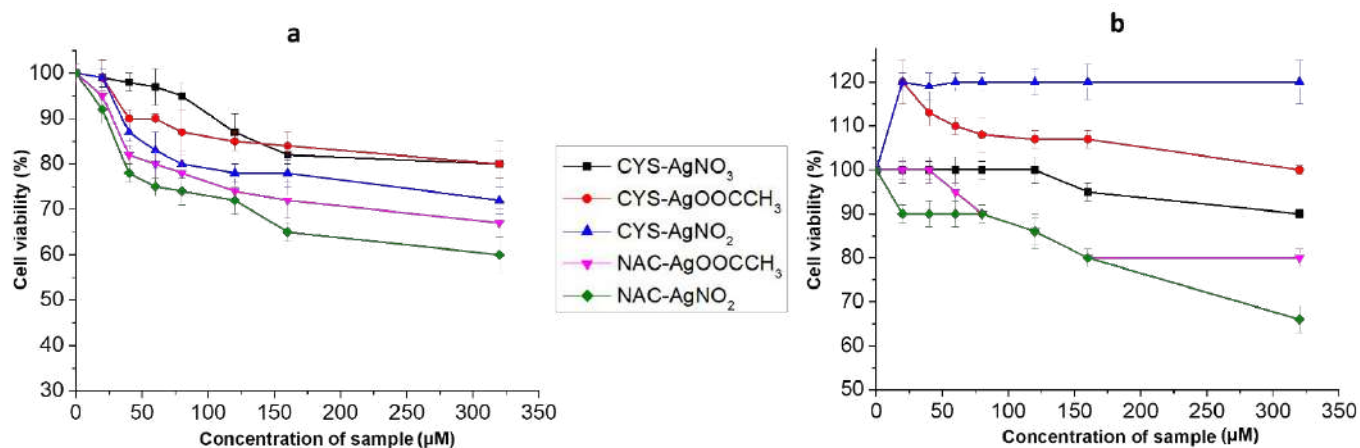


Fig. 6 Cytotoxicity (MTT-test) of CYS-AgNPs and NAC-AgNCs systems to the Wi-38 fibroblast cells (a) and macrophages (b). Wi-38 and macrophage cells incubation with systems is 48 h.

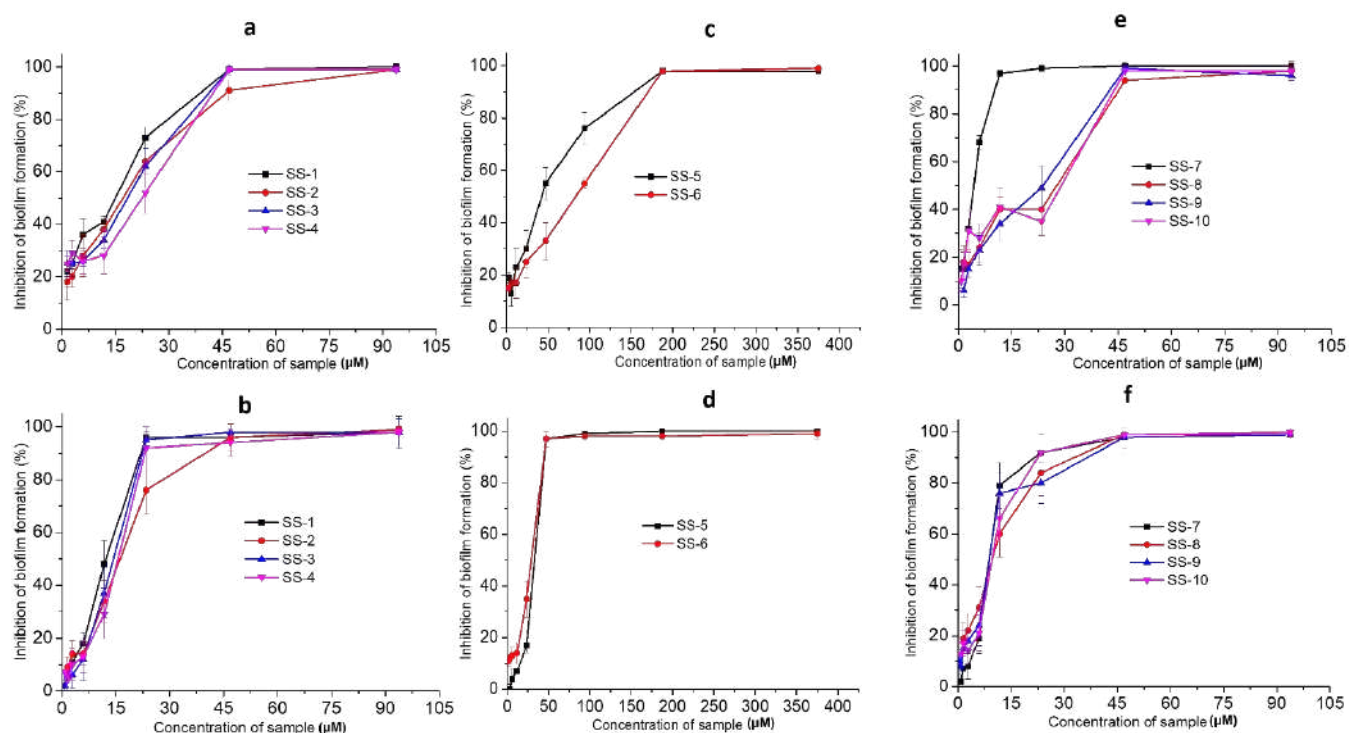


Fig. 7 Antibiofilm activity of SS-1 – SS-10 samples against *P. aeruginosa* (Top) and *A. baumannii* (Bottom): a,b,c,d – CYS-AgNPs and e,f - NAC-AgNCs systems.

therapy. All samples did not cause the lysis of erythrocytes (Table S2). Systems showed low cytotoxicity to fibroblasts and macrophages, its values didn't exceed IC_{50} . The NAC systems were a little more toxic than CYS. Interestingly, some of CYS systems promote macrophages proliferation even at high concentration of the sample. This effect can be connected with the amino acids influence.

Since SS-1 – SS-10 systems showed the highest activity in relation to gram-negative bacteria, studies of their antibiotic film properties were carried out on appropriate bacterial films (Fig. 7). Furthermore, *P. aeruginosa* and *A. baumannii* are the most prominent at forming biofilms amongst the tested in this work and other known bacteria. The activity of samples grows in a row: CYS-AgNO₂ (SS-5, SS-6) < CYS-AgNO₃ and CYS-AgOOCCH₃ (SS-1 – SS-4) < NAC-AgNO₂ (SS-9, SS-10) <

NAC-AgOOCCH₃ (SS-7, SS-8). In all cases NAC systems suppressed the formation of biofilms twice as much as CYS ones for both line of bacterial strains. Herewith, NAC-AgOOCCH₃ (SS-7) turned out to be the most active among all samples and inhibited the biofilms formation at 1×MIC whereas other samples made it from 2×MIC to 4×MIC. It should be noted the SS-7 had a quite low cytotoxicity to normal cells even at concentrations an order of magnitude higher than MIC. The lower toxicity of NAC-AgOOCCH₃ compared to NAC-AgNO₂ can be connected with the more toxic effect of nitrite ions opposed to acetate ones.

According to the proposed structure of nanoparticles (Fig. 5) their surface has positive and negative charge values in CYS-AgX and NAC-AgX systems respectively in the initial solutions (pH<7). But at

conditions of the experiment which corresponds to physiological (pH 7.2-7.4) the equilibrium of the protolytic dissociation shifts towards the formation of $-NH_2$ groups in CYS ($-NH-COCH_3$ in NAC) and COO^- in both systems. Particles surface is charged negatively. The bacterial membrane has a negative charge in the range of -10 to -50 mV of zeta-potential values in dependence of the type of bacteria.⁶³ Thus, the probability of direct binding of nanoparticles to the bacterial membrane surface is unlikely. Although, there are several works where negatively charged AgNPs showed the strong antibacterial effect.^{63,64} We reckon that at pH>7 nanoparticle shell, consisting of CYS/Ag⁺ or NAC/Ag⁺ complexes, start destroying due to the repulsion of fully deprotonated negatively charged carboxylic groups that leads to breaking of hydrogen bondings (Fig. 5). Silver-sulfur bonds in complexes are seemed also broken down. As a result, there are a release of silver ions and cores of AgNPs or AgNCs. These species react with thiol-containing proteins of bacterial membrane because of the high affinity of silver to sulphur or cause ROS thereby disrupting it functions and leading to the death of bacteria. Herewith AgNCs are more active than AgNPs due to their smaller size and greater mobility. Moreover, according to Ostwald-Freundlich equation, smaller silver particles are more susceptible to the release of Ag⁺ ions owing to their greater surface area. If the initial nanoparticles are able to penetrate the membrane of bacteria, then NAC systems will make it easier due to the smaller hydrodynamic particle sizes. Concerning inhibitory ability of systems to biofilms formation the additional and important influence may also have amino acids since it is known, L-cysteine and more N-acetyl-L-cysteine possess antibiofilm activity in the concentration range of 0,01 – 0,5 M.^{65,66} This effect is dealt with the possibility of CYS and NAC thiol-groups partaking in the thiol-disulfide exchange and thus destructing of -S-S- bonds which are responsible for stabilizing the hydrophobic surface of biofilms.⁶⁷ Indeed, after destruction of CYS/Ag⁺ and NAC/Ag⁺ complexes and releasing of Ag⁺, free CYS and NAC moieties form with protonated thiol-group (pK_a (SH) = 9.52). The elucidation of the mechanism of interaction of investigated systems with bacteria and biofilms as well as carrying out *in vivo* experiments is the subject of further research.

Conclusions

In this work nanosilver-based sols and hydrogels with core-shell like structure of particles were prepared using the L-cysteine and N-acetyl-L-cysteine as bio-reducing agents at ambient conditions without any additional components or other exposures. The chemical nature of the amino acid dramatically influenced the final microstructure of resulting materials that is obtaining of silver nanoparticles and silver clusters in the case of CYS and NAC respectively. This peculiarity defined stronger antibacterial and antibiofilm properties of NAC-based systems then CYS ones. Therefore, the novel CYS-AgNPs and NAC-AgNCs systems obtained via the simple “green” chemistry technique can be potentially used as alternative materials against various bacterial infections mediated by biofilms formation.

Author Contributions

Results were interpreted and the manuscript was written by D.V.V. D.V.V. supervised all the structural experiments. The synthesis and physicochemical analysis were carried out by D.V.A. and D.V.V. Microscopic studies were performed by A.A.E. and A.A.L. MTT-test data were received by A.R.M. Hemolysis, antibacterial and biofilms formation assays were performed by E.V.V. and M.S.S. under supervision of O.V.S. All authors have given approval to the final version of the manuscript and declare no competing financial interest.

Conflicts of interest

There are no conflicts to declare.

Acknowledgements

This work was carried out with the financial support of Russian Science Foundation № 21-73-00134 on the equipment of the Shared Facility Centre of Tver State University.

Notes and references

- 1 M. Assefa, A. Amare, *Infect. Drug Resist.*, 2022, **15**, 5061-5068.
- 2 J.L. Del Pozo, *Expert Rev. Anti-Infect. Ther.*, 2018, **16**, 51-65.
- 3 C.A. Arias, B.E. Murray, *N. Engl. J. Med.*, 2015, **372**, 1168-1170.
- 4 D. Sharma, L. Misba, A.U. Khan, *Antimicrob. Resist. Infect. Control*, 2019, **8**, 76-86.
- 5 A. Ghosh, N. Jayaraman, D. Chatterji, *ACS Omega*, 2020, **5**, 3108-3115.
- 6 F. Cui, T. Li, D. Wang, S. Yi, J. Li, X. Li, *J. Hazard. Mater.*, 2022, **431**, 1285-1297.
- 7 L.D. Blackman, Y. Qu, P. Cass, K.E.S. Locock, *Chem. Soc. Rev.*, 2021, **50**, 1587-1616.
- 8 S. Qayyum, A.U. Khan, *Med. Chem. Comm.*, **7**, 1479-1498.
- 9 K. McNamara, S.A.M. Tofail, *Adv. Phys-X*, 2017, **2**, 54-88.
- 10 M. Jiao, P. Zhang, J. Meng, Y. Li, C. Liu, X. Luo, M. Gao, *Biomater. Sci*, 2018, **6**, 726-745.
- 11 A.-C. Burdusel, O. Gherasim, A.M. Grumezescu, L. Mogoanta, A. Ficai, E. Andronescu, *Nanomaterials*, 2018, **8**, 681-705.
- 12 A. Roy, O. Bulut, S. Some, A.K. Mandal, M.D. Yilmaz, *RSC Adv.*, 2019, **9**, 2673-2702.
- 13 L. Xu, Y.-Y. Wang, J. Huang, C.-Y. Chen, Z.-X. Wang, H. Xie, *Theranostics*, 2020, **10**, 8996-9031.
- 14 K.R.B. Singh, V. Nayak, J. Singh, A.K. Singh, R.P. Singh, *RSC Adv.*, 2021, **11**, 24722-24746.
- 15 A. Nicolae-Maranciuc, D. Chicea, L.M. Chicea, *Int. J. Mol. Sci.*, 2022, **23**, 5778-5808.
- 16 S.H. Lee, B.-H. Jun, *Int. J. Mol. Sci*, 2019, **20**, 865-888.
- 17 L.E. Valenti, C.E. Giacomelli, *J. Nanopart. Res.*, 2017, **19**, 156-165.
- 18 S. Shankar, J.-W. Rhim, *Carbohydr. Polym.*, 2015, **130**, 353-363.
- 19 R.A. Matos, L.C. Courrol, *Amino Acids*, 2017, **49**, 379-388.
- 20 D.I. Saragih, D.C.V. Arifin, B. Rusdiarso, S. Suyanta, S.J. Santos, *Key Eng. Mat.*, 2019, **840**, 360-367.
- 21 D.V. Vishnevskii, A.R. Mekhtiev, T.V. Perevozova, A.I. Ivanova, D.V. Averkin, S.D. Khizhnyak, P.M. Pakhomov, *Soft Matter*, 2022, **18**, 3031-3040.
- 22 D.V. Vishnevskii, A.R. Mekhtiev, T.V. Perevozova, D.V. Averkin, A.I.

- Ivanova, S.D. Khizhnyak and P.M. Pakhomov, *Soft Matter*, 2020, **16**, 9669-9673.
- 23 D.V. Vishnevetskii, A.I. Ivanova, S.D. Khizhnyak, P.M. Pakhomov, *Fibre Chemistry*, 2021, **53**, 5-10.
- 24 D.I. Belenkii, D.V. Averkin, D.V. Vishnevetskii, S.D. Khizhnyak, P.M. Pakhomov, *Measurement Techniques*, 2021, **64**, 328-332.
- 25 D.V. Vishnevetskii, D.V. Averkin, A.A. Efimov, A.A. Lizunova, A.I. Ivanova, P.M. Pakhomov, E. Ruehl, *Soft Matter*, 2021, **17**, 10416-10420.
- 26 K. Zheng, X. Yuan, N. Goswami, O. Zhang, J. Xie, *RSC Adv.*, 2014, **4**, 60581-60596.
- 27 Y.-P. Xie, Y.-L. Shen, G.-X. Duan, J. Han, L.-P. Zhang, X. Lu, *Mater. Chem. Front.*, 2020, **4**, 2205-2222.
- 28 Y. Xia, D. J. Campbell, *J. Chem. Educ.* 2007, **84**, 91-96.
- 29 J.C. Fuentes, J. Rivas, M.A. Lopez-Quintela, *Encycl. Nanotechnol*, 2011, 1-15.
- 30 K.V. Mrudula, T.U.B. Rao, T. Pradeep, *J. Mater. Chem.*, 2009, **19**, 4335-4342.
- 31 X. Yuan, M.I. Setyawati, D.T. Leong, J. Xie, *Nano Res.*, 2013, **7**, 301-307.
- 32 X.-R. Song, N. Goswami, H.-H. Yang, J. Xie, *Analyst*, 2016, **141**, 3126-3140.
- 33 C.P. Joshi, M.S. Bootharaju, M.J. Alhilaly, O.M. Bakr, *J. Am. Chem. Soc.*, 2015, **137**, 11578-11581.
- 34 A.M. Perez-Marino, M.C. Blanco, D. Buceta, M.A. Lopez-Quintela, *J. Chem. Educ.*, 2019, **96**, 558-564.
- 35 X.L. Guével, C. Spies, N. Daum, G. Jung, M. Schneider, *Nano Res.*, 2012, **5**, 379-387.
- 36 L. Dhanalakshmi, T. Udayabhaskararao, T. Pradeep, *Chem. Commun.*, 2012, **48**, 859-861.
- 37 E. Khatun, A. Ghosh, D. Ghosh, P. Chakraborty, A. Nag, B. Mondal, S. Chennu, T. Pradeep, *Nanoscale*, 2017, **9**, 8240-8248.
- 38 L.G. AbdulHalim, N. Kothalawala, L. Sinatra, A. Dass, O.M. Bakr, *J. Am. Chem. Soc.*, 2014, **136**, 15865-15868.
- 39 R. Jin, C. Zeng, M. Zhou, Y. Chen, *Chem. Rev.*, 2016, **116**, 10346-10413.
- 40 I. Chakraborty, T. Pradeep, *Chem. Rev.*, 2017, **117**, 8208-8271.
- 41 J. Yan, B.K. Teo, N. Zheng, *Acc. Chem. Res.*, 2018, **51**, 3084-3093.
- 42 T.V. Potapenkova, D.V. Vishnevetskii, A.I. Ivanova, S.D. Khizhnyak, P.M. Pakhomov, *Russ. Chem. Bull.*, 2022, **71**, 2123-2129.
- 43 B. Sharma, M.K. Rabinal, *J. Alloys Compd.*, 2015, **649**, 11-18.
- 44 Z. Chen, Y. Shen, A. Xie, J. Zhu, Z. Wu, F. Huang, *Cryst. Growth Des.*, 2009, **9**, 1327-1333.
- 45 J.I. Hussain, S. Kumar, A.A. Hashmi, Z. Khan, *Adv. Matt. Lett.*, 2011, **2**, 188-194.
- 46 A.S. Prakasha Gowda, A. Schaefer, T. Schuck, *Cell and Gene Therapy Insights*, 2020, **6**, 303-323.
- 47 R. A. Bell, *Environ. Toxicol. Chem.*, 1999, **18**, 9-22.
- 48 J.-S. Shen, D.-H. Li, M.-B. Chang, J. Zhou, H. Zhang, Y.-B. Jiang, *Langmuir*, 2011, **27**, 481-486.
- 49 R. Randazzo, A. D. Mauro, A. D'Urso, G. C. Messina, G. Compagnini, V. Villari, N. Micali, R. Purrello and M. E. Fragala, *J. Phys. Chem. B*, 2015, **119**, 4898-4904.
- 50 B. O. Leung, F. Jalilehvand, V. Mah, M. Parvez, Q. Wu, *Inorg. Chem.*, 2013, **52**, 4593-4602.
- 51 C. Zhang, K. Wang, C. Li, Y. Liu, H. Fu, F. Pan, D. Cui, *J. Mat. Chem. B*, 2014, **2**, 6931-6938.
- 52 D. Li, B. Kumari, J.M. Makabenta, B. Tao, K. Qian, X. Mei, V.M. Rotello, *J. Mat. Chem. B*, 2020, **8**, 9466-9480.
- 53 Z. Ye, H. Zhu, S. Zhang, J. Li, J. Wang, E. Wang, *J. Mat. Chem. B*, 2021, **9**, 307-313.
- 54 K. Wang, Y. Wu, H. Li, M. Li, D. Zhang, H. Feng, H. Fan, *RSC Adv.*, 2014, **4**, 5130-5135.
- 55 J.H. Priester, A. Singhal, B. Wu, G.D. Stucky, P.A. Holden, *Analyst*, 2014, **139**, 954-963.
- 56 B.R. Khalkho, R. Kurrey, M.K. Deb, K. Shrivastava, S.S. Thakur, S. Pervez, V.K. Jain, *Helv. Chim. Acta*, 2020, **6**, e03423.
- 57 S. Panhwar, S.S. Hassan, R.B. Mahar, A. Canlier, M. Arain, *J. Inorg. Organomet. Polym. Mater.*, 2018, **28**, 863-870.
- 58 S. Mandal, A. Gole, N.L. Rajesh, V. Ganvir, M. Sastry, *Langmuir*, 2001, **17**, 6262-6268.
- 59 H. Liu, Y. Ye, J. Chen, D. Lin, Z. Jiang, Z. Liu, B. Sun, L. Yang, J. Liu, *Chem. Eur. J.*, 2012, **18**, 8037-8041.
- 60 S.A. Ahmad, S.S. Das, A. Khatoon, M.T. Ansari, M. Afzal, M.S. Hasnain, A.K. Nayak, *Mater. Sci. Energy Technol.*, 2020, **3**, 756-769.
- 61 T. Chatterjee, B.K. Chatterjee, D. Majumdar, P. Chakrabarti, *Biochim. Biophys. Acta.*, 2015, **1850**, 299-306.
- 62 M. Akter, Md.T. Sikder, Md.M. Rahman, A.K.M. Ullah, K.F.B. Hossain, S. Banik, T. Hosokawa, T. Saito, M. Kurasaki, *J. Adv. Res.*, 2018, **9**, 1-16.
- 63 A.P.V. Ferreyra Maillard, J.C. Espeche, P. Maturana, A.C. Cutro, A. Hollmann, *BBA Biomembranes*, 2021, **1863**, 183597.
- 64 L. Salvioni, E. Galbiati, V. Collico, G. Alessio, S. Avvakumova, F. Corsi, P. Tortora, D. Prospero, M. Colombo, *Int. J. Nanomedicine*, 2017, **12**, 2517-2530.
- 65 G. Zara, M.B. Zeidan, F. Fancello, M.L. Sanna, I. Mannazzu, M. Budroni, S. Zara, *Appl. Microbiol. Biotechnol.*, 2019, **103**, 7675-7685.
- 66 F. Blasi, C. Page, G.M. Rossolini, L. Pallecchi, M.G. Matera, P. Rogliani, M. Cazzola, *Respiratory Medicine*, 2016, **117**, 190-197.
- 67 B. Pedre, U. Barayeu, D. Ezerina, T.P. Dick, *Pharmacology and Therapeutics*, 2021, **228**, 107916.

Table of contents entry

L-cysteine and N-acetyl-L-cysteine mediated synthesis of nanosilver-based sols and hydrogels with antibacterial and antibiofilm properties

Dmitry V. Vishnevetskii,^{a} Dmitry V. Averkin,^{a,b} Alexey A. Efimov,^c Anna A. Lizunova,^c Olga V. Shamova,^d Elizaveta V. Vladimirova,^d Maria S. Sukhareva^d and Arif R. Mekhtiev^e*

^aDepartment of Physical Chemistry, Tver State University, Tver 170100, Russia.

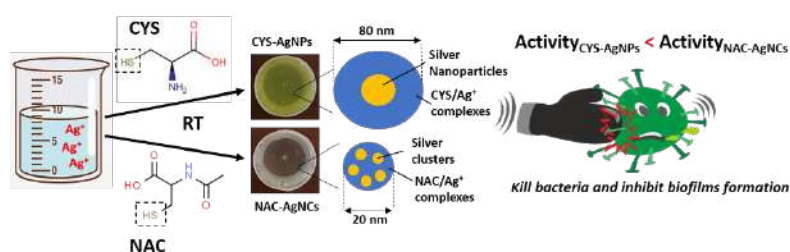
^bRussian metrological institute of technical physics and radio engineering, Moscow 141570, Russia

^cMoscow Institute of Physics and Technology, National Research University, Dolgoprudny 141701, Russia

^dWorld-Class Research Center “Center for Personalized Medicine”, Institute of Experimental Medicine, St. Petersburg 197376, Russia

^eInstitute of Biomedical Chemistry, Moscow 119121, Russia

*Correspondence: rickashet@yandex.ru (D.V.V.)



Novel silver-based materials with enhanced antibacterial and antibiofilm activity were prepared using the **L-cysteine and N-acetyl-L-cysteine** as a bio-reducing agents and silver salts **at ambient conditions without any additional components or other exposures.**

Referee 1:

- 1. Question:** The authors think this work could open the perspectives in medicine, therefore the animal assays and results should provide.

Answer: This work was performed within the framework of the Russian Science Foundation (RSF) grant and its ultimate goal was to identify the most promising samples based on the results of *in vitro* experiments. Next, we intend to carry out *in vivo* experiments in collaboration with our colleagues from the Institute of Experimental Medicine, having previously received funding from the RSF.

- 2. Question:** In Fig.2, please provide the name of Y axis.

Answer: Thank you for this remark, the name (Absorbance) of Y axis have been added.

- 3. Question:** In Fig.6b, please explain why the cell viability of CYS-AgOOCCH₃ and CYS-AgNO₂ is above 100%?

Answer: This fact can be connected with the generation of the free amino acid at experimental conditions which is a nutrient medium for normal cells and the difference between proposed particles structure for CYS-AgX and NAC-AgX systems: AgNPs are less toxic than AgNCs. Furthermore, macrophages are the cells of the innate immune system and they are more resistant to various foreign and toxic substances compared to fibroblasts, for instance.

- 4. Question:** In Fig.7, why the inhibition of biofilm formation of SS-10 decreased at 30 μ M compared with 20 μ M? And the six graphs should added the A,B,C.

Answer: I think this is simply due to the error of the experiment, but this error is included in the confidence interval. A-F marks have been added.

Referee 2:

Dear reviewer,

Thank you very much for the detailed analysis of our manuscript!

- 1. Question:** The motivation and novelty of this work as compared to previous findings from the Authors should be more clearly stated. The concepts of the Introduction reported at page 2, left column, shows close similarities with those presented in ref 40 by the Authors (page 3031, 3032). Also, at the end of page 2 (Introduction, left column) it is said that the scope of the present work is to investigate aspect such as toxicity,... relationship between their structure and properties... which have not been investigated so far. This doesn't seem to be entirely the case (see also ref. 40 by the Authors), so please revise the text/motivation of the work accordingly. [Please check-Data presented in Fig 4 c,d were already presented in ref 40?]. Overall, the manuscript should present more clearly the relevant features (see also point 2) and novelty of the investigation as compared to previous work.

Answer: Yes, you are absolutely right. I have rewritten the introduction part.

- 2. Question:** At page 6, 7 the proposed architecture of the investigated materials is described: the obtained composites present either Ag nanoparticles or Ag clusters embedded within CYS- or NAC-based hydrogel containing CYS/Ag⁺ or NAC/Ag⁺ complexes (together with the counterion of the silver precursor and the ions used as gelators, as far as I understand). To improve the clarity of the manuscript, I suggest to make clear in the text (for example in

the abstract, and earlier in the results and discussion) the composite nature of the produced materials. Regarding the “core” of the composites, a significant difference is observed in CYS vs NAC systems, as nanocrystalline Ag is obtained in the first case which is not observed in the latter. I suggest that the oxidation state of silver is investigated to gain insights on the reducing role of CYS and NAC.

Answer: I have rethought this question and concluded that it doesn't correct to use word «composite» in our case because of we talk about the composite structure of particles but not about the final material as a composite. So, I have revised it. Concerning the oxidation state of silver, I think only XPS analysis can give the clearest results and we intend to perform such experiments with our colleagues from Moscow Institute of Physics and Technology, but they have some problem with their equipment since something was broken down. This problem is getting more complicated by sanctions due to the fact that all repair parts are purchased abroad.

3. **Question:** Although I am not an expert in the field, the presented data seem to point at a significant activity in bacteria suppression and biofilm inhibition, where the NAC samples show improved properties as compared to CYS samples. The Authors conclude (pag 9) that NAC samples are more active due to the speculated occurrence of Ag clusters as opposed to Ag nanoparticles in the core. My advice is that the Authors should provide further support to this view, as bioactivity is also expected from the CYS/Ag⁺ or NAC/Ag⁺ complexes in the outer layer of the composite. In addition the Authors suggest that also the anion arising from the silver precursor can play a role to some extent, so my advice is that a comment on how to entangle the different contributions in order to compare the different bioactivities recorded for the CYS and NAC samples is needed.

Answer: In the present article we have only put forward the proposed mechanism of particles interaction with planktonic bacteria and biofilms including the role of CYS/Ag⁺ and NAC/Ag⁺ complexes (page 9, below). To verify the proposed mechanism, we plan to carry out experiments in the future where we will add Ellman's reagent (we have ordered it and waiting for) to our samples at physiological conditions to check out the presence of the free SH-groups. The control experiment will be fixing of the released Ag⁺ by ion-selective electrode.

4. **Question:** Is there any reason why the samples were not investigated by X-ray diffraction?

Answer: We have tried to do the XRD for our samples but the concentration of the solid phase is quite low (0,01%). And we observed just wide peak throughout the spectra. Though in our related article [1] we have managed to fix the diffraction peaks corresponding to the crystalline phase of AgNPs, but only in the case of the final composite material. XRD peaks were widened that point to quite amorphous state of samples and can be connected with the presence of CYS/Ag⁺ and NAC/Ag⁺ complexes in the shell of proposed structure of particles.

5. **Question:** My feeling is that reference to literature could be improved. I suggest that the presentation of previous work in the field of silver nanoparticles and clusters, use of cysteine in the synthesis of metal nanoparticles, and so on is reported in greater detail. (just by means of example, see work by M.A. López-Quintela and coworkers).

Answer: In accordance with the literature, there are a literally several articles related to methods of the synthesis of silver nanoparticles and silver clusters using sulfur-containing amino acids, as well as the study of bioactive properties of obtained compositions (see Table 2, ref. 54-59). I have read the latest works of M.A. López-Quintela and added them in the introduction part of the manuscript (ref. 29 and 34).

References:

1. D.V. Vishnevetskii, D.V. Averkin, A.A. Efimov, A.A. Lizunova, A.I. Ivanova, P.M. Pakhomov, E. Ruehl, *Soft Matter*, 2021, **17**, 10416-10420.

Minor Comments:

M1: The mistakes have been corrected and the sentences have been rephrased. Concerning the «simplest», you are absolutely right, and I have changed «simplest» to «simple».

M2: I agree with you, it has been corrected.

M3: The solutions were filled in polystyrene cuvette without any other manipulations. The gels (thixotropic) were mechanically destroyed just by shaking and diluted by water in 2, 4 and 8 times and placed in polystyrene cuvette. DLS can't give the correct information for gels only for Newtonian liquids. The dilution in 2, 4 and 8 times was needed for checking out the stability of the system, we observed that the average hydrodynamic diameter didn't change at diluting.

M4: Certainly, thank you! It has been changed.

M5: This is the standard abbreviations, but anyway I have defined some of them.

M6: The information has been added.

M7: See M3.

M8: We did not study the chemical nature of these precipitates but it is probably the silver mercaptide. We will try to find it out by XRD and XPS analysis in the future.

L-cysteine and N-acetyl-L-cysteine mediated synthesis of nanosilver-based sols and hydrogels with antibacterial and antibiofilm properties[†]

Dmitry V. Vishnevetskii,^{a*} Dmitry V. Averkin,^{a,b} Alexey A. Efimov,^c Anna A. Lizunova,^c Olga V. Shamova,^d Elizaveta V. Vladimirova,^d Maria S. Sukhareva^d and Arif R. Mekhtiev^e

Received 00th January 20xx,
Accepted 00th January 20xx

DOI: 10.1039/x0xx00000x

The problem of the synthesis of a new generation of medicines aimed at combating bacteria and biofilms caused various infections is a great urgency. There is a gradual departure from conventional techniques of treatment with the use of antibiotics, and consequently, the search for new methods and approaches for obtaining and rational use of available antibacterial drugs to which microorganisms do not acquire resistance. Although silver nanoparticles (AgNPs) and silver nanoclusters (AgNCs) have exhibited certain effectiveness against multidrug-resistant bacteria and biofilms, there are too few simple, cheap and easy-to-scale methods for AgNPs and AgNCs obtaining with well-desired characteristics. In this work, we have carried out the one-pot synthesis of sols and gels containing AgNPs and AgNCs using the only L-cysteine (CYS) or N-acetyl-L-cysteine (NAC) as bioreducing/capping/gel-forming agents and different silver salts – nitrate, nitrite and acetate. HRTEM, SAED, EDX mapping, AFM, SEM, EDX, ICP-MS and FTIR analysis confirmed the formation of spherical/elliptical CYS-AgNPs and NAC-AgNCs particles consisting of AgNPs or AgNCs “core” and CYS/Ag⁺ or NAC/Ag⁺ complexes “shell” with mean average diameter of 10 and 5 nm respectively. UV-Vis spectroscopy fixed localized surface plasmon resonance (LSPR) at 390–420 nm for CYS-AgNPs systems and LSPR absence for NAC-AgNCs ones. DLS and nanoparticle tracking analysis (NTA) data indicated that mean average diameter of particles is about 80 nm for CYS-AgNPs systems and 20 nm for NAC-AgNCs ones. Zeta potential measurements showed particles possess the positive and negative charge values for CYS-AgNPs and NAC-AgNCs systems respectively. The prepared materials demonstrated the high antibacterial activity against the most common types of bacteria at MIC range of 10–100 μM, wherein, the effect of NAC-AgNCs systems in 2 times stronger than CYS-AgNPs ones. The both systems are non-toxic/low-toxic at 300 μM for the normal human cells: erythrocytes, fibroblasts and macrophages. Sols and hydrogels in concentration range of 20–40 μM showed the complete inhibition of formation of biofilms *Acinetobacter baumannii* and *Pseudomonas aeruginosa* belonging to ESKAPE pathogens group and representing the most serious problem in practical medicine. NAC-AgNCs systems were the most active. The simple strategy of the preparation of AgNPs/AgNCs-based sols and gels along with their pronounced antibacterial and antibiofilm activity could open the perspectives for its applications in medicine.

Introduction

The multidrug-resistant bacteria and especially biofilms are cause of the various infections: more than 65% of nosocomial, 80% of chronic and 60% of all human bacterial ones.¹ Biofilm-associated diseases increase the human morbidity and mortality rates and economic burdens because of high healthcare costs and prolonged patient stays.² Although antibiotics were the main antibacterial drugs in the

past century, their frequent and excessive use lead to the extensive multidrug resistance.³ The problem is complicated by the fact that biofilms are inherently insensitive to antibiotics and are upwards of 1000-fold more resistant to them than planktonic bacteria.⁴ Thus, the search and development of an effective and safe medicines against bacteria and biofilms is a great challenge. There have been extensive studies related to the creation of new materials for the elimination of biofilms using small molecule agents,⁵ carbon nanomaterials⁶, macromolecular species⁷ and inorganic nanoparticles.⁸ The latter have a significant place in the field of biomedical applications due to a unique range of properties: antibacterial, anticancer, magnetic, optoelectrical, biosensing, bio-imaging and etc.^{9,10} Among of them silver nanoparticles (AgNPs) are one of the promising candidates in the therapy of the different infectious diseases and medical devices owing to their broad-spectrum antibacterial activity and little drug resistance.^{11–15} It has been shown that properties of AgNPs – cytotoxicity and bioactivity directly depend on their characteristics: size, distribution, morphological shape and surface charge.¹⁶ Furthermore, AgNPs can

^aDepartment of Physical Chemistry, Tver State University, Tver 170100, Russia.

E-mail: rickashet@yandex.ru

^bRussian metrological institute of technical physics and radio engineering, Moscow 141570, Russia

^cMoscow Institute of Physics and Technology, National Research University, Dolgoprudny 141701, Russia

^dWorld-Class Research Center “Center for Personalized Medicine”, Institute of Experimental Medicine, St. Petersburg 197376, Russia

^eInstitute of Biomedical Chemistry, Moscow 119121, Russia

[†]This work is dedicated to prof. Maxim M. Ovchinnikov and Nadezhda A. Vishnevetskaya.

^{††}Electronic Supplementary Information (ESI) available: UV, HRTEM, SAED, EDX mapping, SEM, EDX, AFM, ICP-MS, DLS, NTA, Zeta-potential measurements, FTIR, Antibacterial assay, Hemolysis assay, MTT-test See DOI: 10.1039/x0xx00000x

easily agglomerate and oxidize that leads to suppression of their antibacterial and antibiofilm capacities.¹⁷ Hence, the practical applications of AgNPs need to use the biocompatible and either non-toxic or low-toxicity synthetic protocols along with remaining of the high activity of obtained AgNPs.

We have lately mentioned about various biological approaches which use "green" nanotechnologies for AgNPs synthesis, considered their disadvantages and come to conclusion that one of the best ways is to use the low molecular weight bio-reducing agent without any other related components in its initial solution, for instance, amino acids.¹⁸⁻²¹ We have shown that L-cysteine (CYS) can simultaneously act as a reducing, capping and gel-forming agent at the simplest mixing of its aqueous solution with silver salts at ambient conditions.²¹⁻²⁵ As a result of the research, we have previously found out that the surface state and the size of obtained nanoparticles directly determine the ability of the system to form a gel, as well as the properties of the final material: anticancer, catalytic, electrochemical, film-forming.

The number of articles which is devoted to the production and application of silver nanoparticles grow every year, while recently there has been more and more information about the synthesis and various properties of silver nanoclusters (AgNCs).^{26,27} It is well known that some of metal nanoparticles possess the characteristic absorption band in the UV spectrum, called localized surface plasmon resonance (LSPR), occurring due to a coherent and collective oscillation of the electrons on the nanoparticle surface when interacting with light of a wavelength much bigger than the particle size.²⁸ The picture absolutely changes in the case of AgNCs: no LSPR observed since all conducting electrons are now quantized, losing all metallic properties because of quite small sizes of particles.²⁹

AgNCs have demonstrated some superior properties over AgNPs. They possess stronger bioactive effect (antibacterial, anticancer and etc.) compared to AgNPs due to their less size.^{30,31} This fact, besides, determines less toxicity of AgNCs even in the *in vivo* experiments. For instance, they penetrate through the kidney barrier much better opposed to AgNPs and it allows them to be efficiently cleared from the body without causing serious damage.³²

There are several strategies for AgNCs synthesis such as direct reduction,^{33,34} chemical etching^{35,36} and ligand exchange.^{37,38} Organic ligands such as thiolates, phosphines, and alkynyls are usually used to cap on the surface in order to prevent aggregation and to facilitate the isolation of target AgNCs.³⁹⁻⁴¹ However, all of these approaches are quite expensive and (or) toxic reagents are used, consequently it can't be easy scalable, safe for humans and environment.

In the present article, we delved into the study of the self-assembly process with partaking of sulfur-containing amino acids and silver salts. To do this, firstly, we used additional methods for analyzing the structure of obtained nanoparticles, and, secondly, for the first time, we investigated in detail the behavior of systems obtained at mixing of N-acetyl-L-cysteine (NAC) aqueous solutions with silver salts. NAC is well-known available mucolytic, expectorant, antioxidant agent. An unexpected result was that the replacement of CYS with NAC lead to the formation of non-crystalline silver phase – silver clusters. This system turned out to be twice more active in planktonic bacteria suppression and more importantly their biofilms in *in vitro* experiments. CYS-AgNPs and NAC-AgNCs were non-toxic or

have the low toxicity to the normal human cells in culture. Thus, the novel "green" chemistry approach could open perspectives for the silver-related materials production with the enhanced desired properties.

Experimental

Chemicals

L-cysteine (>99 %) and N-acetyl-L-cysteine (>98 %) were obtained from Acros. Silver nitrite (>99 %), silver nitrate (>99 %) and silver acetate (>99 %) were purchased from Lancaster. All chemicals were used as received. All solutions were prepared on de-ionized water after its filtration on 0.45 μm filters.

General procedure for the preparation of CYS-AgNPs and NAC-AgNCs systems

The solutions (2 mL) were prepared by the following scheme (as an example): the empty vessel 0.8 mL of the de-ionized water was filled, then 0,6 mL of L-cysteine or N-acetyl-L-cysteine (0.01 M) was added, finally 0.6 mL of silver salt (0.01 M) was added (Table 1). 0.15 mL of Na₂SO₄ (0,01 M) as a gelation agent was added in SS-1 and SS-3 samples. The resulting mixtures were stirred at room temperature (25°C) for 1 minute and solutions were stayed in dark place for 3 hours. As a result, from uncolored to yellow or brown transparent solutions or hydrogels were obtained.

Table 1 The synthetic protocol for CYS-AgNPs and NAC-AgNCs systems.

Abbr. of sample	Sample	Water, mL	Amino acid, mL	Silver salt, mL
SS-1	CYS-AgNO ₃	0.65	0.6	0.75
SS-2	CYS-AgNO ₃ -SO ₄ ²⁻	0.65	0.6	0.75
SS-3	CYS-AgOOCCH ₃	0.65	0.6	0.75
SS-4	CYS-AgOOCCH ₃ -SO ₄ ²⁻	0.65	0.6	0.75
SS-5	CYS-AgNO ₂	0.8	0.6	0.6
SS-6	CYS-AgNO ₂	0.65	0.6	0.75
SS-7	NAC-AgOOCCH ₃	0.8	0.6	0.6
SS-8	NAC-AgOOCCH ₃	0.65	0.6	0.75
SS-9	NAC-AgNO ₂	0.8	0.6	0.6
SS-10	NAC-AgNO ₂	0.65	0.6	0.75

HRTEM, SAED and EDX mapping analysis

The microstructure and elemental mapping analysis of the samples were analyzed using a transmission electron microscope JEM-2100 (JEOL Ltd.), equipped with the energy dispersive X-ray spectrometer X-MAXN OXFORD instruments, with an accelerating voltage of up to 200 kV. Samples were placed on a standard copper grid with a 100 nm thick Formvar (polyvinylformal) polymer support, dried, and placed in the microscope.

AFM analysis

The surface topography of the samples was investigated by using a

scanning probe microscope Solver Next (NT-MDT) in the semi-contact mode.

SEM and EDX

The microstructure and chemical composition of the samples were also studied using a raster JEOL 6610 LV electron microscope (JEOL Ltd.) with x-ray system energy dispersive microanalysis Oxford INCA Energy 350. in a high vacuum mode with accelerating voltage of 15 kV. **Samples preparation was consisted of its spraying on the surface of a thin conductive layer of platinum and drying in vacuum (10^{-4} Pa).**

UV-Vis spectroscopy

Electronic spectra of the samples were recorded on the UV spectrophotometer Evolution Array (Thermo Scientific) in a quartz cell with a 1 mm path length.

DLS and zeta potential measurements

Measurement of intensity of light scattering in the studied samples was carried out using analyzer Zetasizer Nano ZS (Malvern) with He-Ne laser (633 nm), power of 4 mW. **The solutions were filled in polystyrene cuvette without any other manipulations.** For the correct analysis of the particle sizes and zeta-potential in gel state, the samples were mechanically destroyed and diluted two, four and eight times. All measurements were carried out at 25°C in the backscattering configuration (173°), providing the highest sensitivity of the device. Mathematical processing of the results of the obtained cross-correlation functions of the diffuse light intensity fluctuations g_2 was carried out in the program Zetasizer Software, where the solution of the obtained equation of the g_2 dependence on the diffusion coefficient was performed by the cumulant method. The result of the solution was the function $z(D)$. The hydrodynamic radii of the scattering particles were calculated from the diffusion coefficients by the Stokes-Einstein formula: $D = kT/6\pi\eta R$, where D is the diffusion coefficient, k is the Boltzmann constant, T is the absolute temperature, η is the viscosity of the medium, R is the radius of the scattering particles. Measurement of the electrophoretic mobility of aggregates in the samples was carried out in U-shaped capillary cuvettes. Zeta potential distributions were calculated using the Henry equation: $UE = 2\epsilon z f(Ka)/3Z$, where UE – electrophoretic mobility, z – zeta potential, ϵ – dielectric constant, Z – viscosity, and $f(Ka)$ – Henry's function, $f(Ka) = 1.5$ for aqueous media.

NTA

The measurements were made with a NanoSight NS300 (Malvern) equipped with a scientific CMOS camera, a 20x objective lens, a blue laser module (405nm, LM12 version C) and NTA software version 3.1. A 1-mL disposable syringe was used to inject the samples into the instrument chamber. For the correct analysis of the particle sizes in gel state, the samples were mechanically destroyed and diluted two, four and eight times. The video data were collected for 30 seconds, repeated three times for each sample. The detection threshold of the NTA software was set to 5 and the maximum jump distance and the minimum track segment length were both set to auto.

ICP-MS analysis

The "PlasmaQuant MS" (Analytik Jena GmbH) mass spectrometer with inductive coupled plasma was used. ICP-MS is equipped with

Scott spray chamber with double passage. The mass spectrometer used argon gas (chemical purity of 99.993%). The sputtering efficiency was determined using a colloidal solution of β -cyclodextrin-stabilized Ag/CDx/W silver nanoparticles with a nominal particle size of 12 nm. The controlled isotope was ^{107}Ag . To quantify the ^{107}Ag intensity in time resolved analysis mode to take ICP-MS data on reconstituted Ag/CDx/W silver nanoparticles diluted to Ag mass fractions from 500 $\mu\text{g/L}$ to 0.25 $\mu\text{g/L}$. Solution of diluted nanoparticles was introduced via peristaltic pump into low-flow (0.7 mL/min) concentric nebulizer and impact bead spray chamber cooled to 2°C. The delay time was set at 3 ms with typical data collection time of 60 s for each measurement.

pH measurements

The pH of the solutions was measured using a Seven Multi S70 (Mettler Toledo) pH meter.

FTIR spectroscopy

FTIR spectra of the samples were recorded on a Vertex 70 spectrometer (Bruker) in the range of 7000–400 cm^{-1} at a resolution of 4 cm^{-1} . The number of scans was 32. The studied samples (solutions and hydrogels) were preliminarily frozen in a liquid nitrogen; the obtained uncolored, yellowish or brown precipitates were carefully washed with de-ionized water and vacuum dried at 25°C. 22 mg of the precipitate was mixed with 700 mg of potassium bromide and pressed into a pellet.

MTT test Wi-38 cells

Wi-38 human normal embryonic lung cells obtained from the American Tissues and Cells Collection (ATCC) were cultivated in 96-well plates at 37°C in atmosphere of 5% CO_2 in a DMEM medium with the addition of L-glutamine (2 mM), antibiotics (100 units per mL of penicillin and 100 $\mu\text{g/mL}$ of streptomycin), and 10% of FBS. The cells were incubated in a serum medium with the tested compounds at various concentrations for 48 h. PBS (10 μL) containing MTT (5 mg/mL) was added to each well, and the cells were incubated at 37°C for 4 h. The culture medium was removed, DMSO (100 μL) was added to each well, a plate was vortex for 20 minutes, and then the optical absorbance in each well was measured at 570 nm in a Multiskan Spectrum Microplate Reader instrument (Thermo Scientific, United States). The MTT test readings were averaged for three independent determinations. Readings of MTT test in the absence of the tested compounds were taken as 100%.

MTT test macrophage cells

The human monocytic leukemia cell line - THP-1 - obtained from ATCC (American Type Culture Collection, Manassas, Virginia) were cultured in RPMI 1640 medium containing 10% fetal bovine serum (FBS), 2 mM L-glutamine, 100 U/mL penicillin, and 100 $\mu\text{g/mL}$ streptomycin (growth medium), at 37°C in an atmosphere containing 5% CO_2 . The cells ($5 \times 10^5/\text{mL}$) were washed and suspended in the same medium, contained phorbol ester (PMA-phorbol 12-myristate-13 acetate (Sigma)) to a final concentration of 100 ng/mL to initiate their transformation into macrophages. The cells ($5 \times 10^3/\text{well}$) were transferred to 96-well plates and incubated for 48 h at 37 °C and 5% CO_2 . Then the cells were incubated in a serum medium with tested compounds at various concentrations for 48 h. PBS (10 μL) containing MTT (5 mg/mL) was added to each well, and the cells were incubated

at 37°C for 4 h. The culture medium was removed, DMSO (100 µL) was added to each well, a plate was vortex for 20 minutes, and then the optical absorbance in each well was measured at 570 nm in a Multiskan Spectrum Microplate Reader instrument (Thermo Scientific, United States). The MTT test readings were averaged for three independent determinations. Readings of MTT test in the absence of the tested compounds were taken as 100%.

Hemolysis assay

Hemolytic activity of samples toward human erythrocytes was determined using a standard protocol (Tossi et al., 1997). Peripheral blood of healthy volunteers was collected into EDTA-coated vacutainer tubes and then repeatedly washed with phosphate-buffered saline (PBS), precooled to 4°C, to remove any trace of plasma components and of anticoagulant. The washing cycle included centrifuging the samples at 300 g at 4°C for 10 min, removing the supernatant and resuspending the cells in a fresh aliquot of PBS. After the third round, 280 mL of cellular precipitate were resuspended with PBS up to 10 mL to obtain a suspension of stock red blood. 90 µL of this stock were mixed with 10 µL of the tested systems, also diluted in PBS to various concentrations; the end concentration of erythrocytes was 2.5% v/v. Mixtures were incubated for 30 min at 37°C and then centrifuged for 3 min at 10,000 g. Hemoglobin release from the lysed erythrocytes was spectrophotometrically measured in the supernatants at 540 nm, using a SpectraMax 250 Spectrophotometer (Molecular Devices, USA). The percentage of hemolysis in test samples was calculated by comparison to a positive control for total hemolysis (100% lysis) where 10 µL of 1% v/v Triton X-100 was used instead of the investigated systems, and with a negative control (0% lysis) where only PBS was added to erythrocytes, according to the following formula:

$$\text{Hemolysis(\%)} = \frac{(OD_{\text{sample}} - OD_{0\% \text{ lysis}})}{(OD_{100\% \text{ lysis}} - OD_{0\% \text{ lysis}})} \times 100\%$$

where OD_{sample} , $OD_{0\% \text{ lysis}}$, and $OD_{100\% \text{ lysis}}$ are respectively the optical density values at 540 nm for the test sample and the negative and positive controls. Experiments were repeated three times and in each case in triplicate (samples and controls). Tests were carried out in accordance with the Declaration of Helsinki, written informed consent was given by all donors beforehand.

Antibacterial Assays

Bacterial strains used were as follows: laboratory strains of *Staphylococcus aureus* ATCC 25923 were kindly provided by Dr. Elena Ermolenko (Institute of Experimental Medicine, St-Petersburg, Russia); drug-resistant bacterial strains *Acinetobacter baumannii* 7226/16 (resistant to imipenem, gentamicin, tobramycin, ciprofloxacin, trimethoprim/sulfamethoxazole), *Pseudomonas aeruginosa* 522/17 MDR (resistant to meropenem, ceftazidime, cefixime, amikacin, gentamicin, netilmicin, ciprofloxacin, colistin), from the urine of patients were generously supplied by Dr. A. Afinogenova from the Research Institute of Epidemiology and Microbiology named after L. Pasteur, Saint Petersburg, Russia; clinical isolate of *Staphylococcus intermedius* (resistant to ciprofloxacin, cefuroxime, clindamycin, erythromycin, rifampicin, gentamicin, benzylpenicillin, and oxacillin) obtained from an infected

wound caused by a dog bite was provided by colleagues from the S.M. Kirov Military Medical Academy (Saint Petersburg, Russia). Initial susceptibility testing was performed by their colleagues from said institutions.

Broth Microdilution Assay

The minimal inhibitory concentrations (MIC) of CYS-AgNPs and NAC-AgNCs systems were determined using microdilution assay in Müller–Hinton (MH) broth in general accordance with the guidelines of the European Committee for Antimicrobial Susceptibility Testing. The procedure is described in (Zharkova et al., 2021). Briefly, two-fold serial dilutions of investigated samples starting with 2 × stock concentration were prepared in sterile phosphate-buffered saline (PBS). Thus, final solutions contained 50% of PBS diluted tested samples and 50% of MH broth with bacteria. Bacteria for testing were grown overnight, then transferred into a fresh portion of 2.1% MH medium and additionally incubated for 2–3 h to obtain bacterial culture in its mid-logarithmic growth phase, which was diluted down to the final concentration of 1×10^6 CFU/mL.

Biofilm Formation Assessment by the Crystal Violet Assay

Quantification of the biofilms forming in the presence of various concentrations of tested systems was performed using the crystal violet assay according to general guidelines (Merritt et al., 2006). Tests were performed in polystyrene 96-well plates with U-shaped bottom. CYS-AgNPs and NAC-AgNCs systems were serially diluted in a bacterial growth medium (MH for *A. baumannii* or TSB for *P. aeruginosa*) in a volume of 50 µL per well. Overnight cultures of tested bacteria in a stationary phase of growth were 50 times diluted and introduced into the experimental wells at the same volume of 50 µL. Samples were incubated for 24 h at 37°C. The content of the wells was then shaken out, the plates were gently washed from unattached planktonic bacteria in still water (poured into a large enough vessel); bacterial cells and matrix components adhered to the walls of the wells were stained with a 0.1% aqueous solution of crystal violet dye: 125 µL of dye solution was put into each well and incubated at room temperature for 10 min. After staining dye solution was removed, the plates were washed with clean water and allowed to air-dry. Finally, the bound dye was redissolved by adding 200 µL of 30% acetic acid into each well, incubating it for 15 min at room temperature, and then thoroughly mixing the content of the wells by pipetting. One hundred and twenty five microliters of crystal violet extract from each well were transferred into a flat-bottomed microtiter plate, and the optical density was measured at a wavelength of 560–595 nm (depending on the maximum of absorption in a particular experiment). Experimental samples were made in quadruplicates, and there were 8–9 repeats of control samples without CYS-AgNPs and NAC-AgNCs systems in each test. Presented results are medians calculated based on 3 independent experiments.

Results and discussion

Synthesis of CYS-AgNPs and NAC-AgNCs systems

In the present study we have synthesized a set of systems by varying

the chemical nature of the silver salt and amino acid, their concentration and ratio based on the results of our preliminary research.²¹ The main idea was to show the similarities and differences of NAC and CYS reaction with various silver salts. At mixing of aqueous solution of CYS and silver salt, regardless of its chemical nature, from yellow-green to brown-colored solutions or thixotropic gels are obtained in the concentration range of the dispersed phase of 1-20 mM (Fig. 1a, Fig. S1,1). In the case of silver nitrate and acetate, the gel formation requires the addition of low molecular weight anions (Cl^- , SO_4^{2-}), whereas for silver nitrite the gel forms without any other components. Some rheological properties and aspects of the gelation mechanism of these systems have been lately studied.²¹ At a fixed concentration of the amino acid, the higher the silver content in the system, the richer the color of the samples. And we have expected the same behavior for NAC. However, one can see that in this case the uncolored solutions are obtained with AgNO_2 and AgOOCCH_3 (Fig. 1b, Fig. S1,2). The interaction of NAC with AgNO_3 gives the white precipitates which is probably dealt with the silver mercaptide formation. The homogeneous samples were SS-1 – SS-10 (Table 1), that's why further we studied mainly these systems. It should be noted that during more 6 months the samples for both – CYS and NAC systems remain stable – no opalescence, precipitation or color changing was fixed. And it was controlled by UV-Vis analysis, DLS and zeta potential measurements. Thus, it is even visually obvious that the behavior of these systems is very different from each other. Therefore, we used an integrated approach to study this phenomenon.

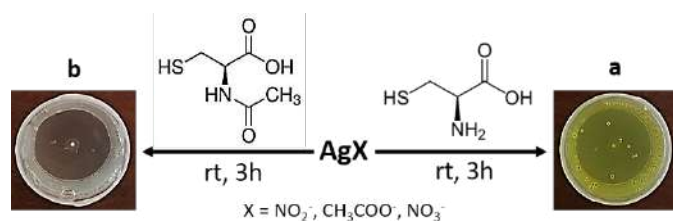


Fig. 1 Scheme of a - CYS-AgNPs and b - NAC-AgNCs systems preparation. $C(\text{CYS}) = C(\text{NAC}) = 3 \text{ mM}$, $C(\text{AgX}) = 3.75 \text{ mM}$ in the final solution.

Characterization of CYS-AgNPs and NAC-AgNCs systems

Since the systems have or haven't the color, one can expect that it must or mustn't absorb quanta of light at a certain wavelength. The principal difference of UV spectra of CYS-AgX and NAC-AgX systems (Fig. 2) is the absence of the absorption band at 390-410 nm for latter one which is responsible for localized surface plasmon resonance (LSPR) of silver nanoparticles.²¹ Widened bands at 280 and 310 nm are attributed to the ligand-to-metal charge-transfer transition (LMCT) and argentophilic interactions in CYS/Ag⁺ complexes respectively.²¹ The growth of the LSPR band and its shift to the region of large wavelengths occurs at increase of the silver content in CYS-AgX systems. Meanwhile, no changes observe for NAC-AgX ones in this region (Fig. 2,a,c). The wide band at 280-310 rises in both systems. The absorption of LSPR band grows at increasing the concentration of the dispersed phase only for CYS-AgX systems and no changes take place for NAC-AgX ones (Fig. 2b,d). It should be noted that at the concentration of the dispersed phase < 1mM LSPR vanished for both systems and samples are uncolored (Fig. S2).

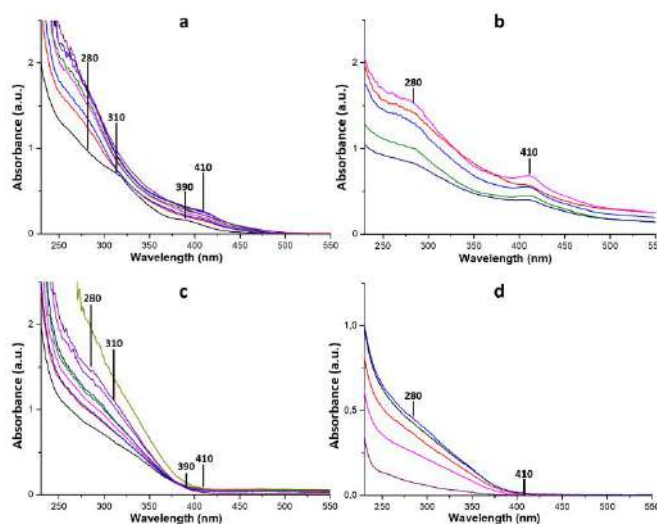


Fig. 2 UV-spectra of a,b - CYS-AgNPs and c,d - NAC-AgNCs systems. a,c - $C(\text{CYS}) = C(\text{NAC}) = 3 \text{ mM}$, $C(\text{AgX}) = 1.5 - 6 \text{ mM}$; b,d - $C(\text{CYS}) = C(\text{NAC}) = 10 \text{ mM}$, $C(\text{AgX}) = 5 - 20 \text{ mM}$.

At higher than 20 mM dispersed phase concentration the white or brown⁴² precipitates are obtained. So, it can be assumed based on the mentioned above data and lately obtained⁴² that the LSPR band is responsible for the color of the samples.

Results obtained by transmission electron microscopy are demonstrated on the Fig. 3 (Fig. S3, S4, S5). The morphology of all systems is the network of filament-like structures constructed from spherical/elliptical nanoparticles of mean average diameter of 5-10 nm. The densest network is observed for CYS-AgNO₂ system (Fig. 3A) because of it forms the gel without any additional components unlike other systems. CYS-AgNO₃ and CYS-AgOOCCH₃ systems can form a gel at initiation by the sulphate-anion (Fig. S5). SAED analysis fixes diffraction rings and reflexes corresponding to 111, 200, 220 and 311 planes of the face-centered cubic lattice of the crystalline phase of silver nanoparticles in the case of CYS-AgX systems and no rings/reflexes for NAC-AgX ones (Fig. 3B, S4). One can also be noted that the increase of the silver salt concentration in CYS-AgX samples leads to rising of the number AgNPs, their sizes and growing of diffraction intensity (Fig. S3). HRTEM shows silver atoms in CYS-AgX systems are close-packed and clear ordered, the interplane distance of 2,33 Å is consistent with the 111 plane of AgNPs (Fig. 3,C,D, S3, S4). This is not taken place for NAC-AgX systems. EDX mapping analysis confirms these data, herewith sulfur atoms are localized on the surface of silver atoms in CYS-AgX systems and both on silver atoms and between them in NAC-AgX ones (Fig. 3,E, S3, S4). These results are in a good agreement with UV analysis data. AFM, SEM, EDX and ICP-MS verify the results of TEM concerning the composition, the character of particle distribution, and their sizes in samples (Fig. S6).

Hydrodynamic and electrokinetic parameters of systems are presented on the Fig. 4 (Fig. S7). Nanoparticles in both systems have the unimodal size distribution that confirms via NTA and DLS. And these methods conform each other. The polydispersity coefficient of particles decreases at moving from CYS to NAC systems. The surface of particles is positively charged in CYS-AgX systems and negatively in NAC-AgX. This is due to the fact that the amino-group is blocked in NAC, thus only the carboxyl group can protonate/deprotonate in this

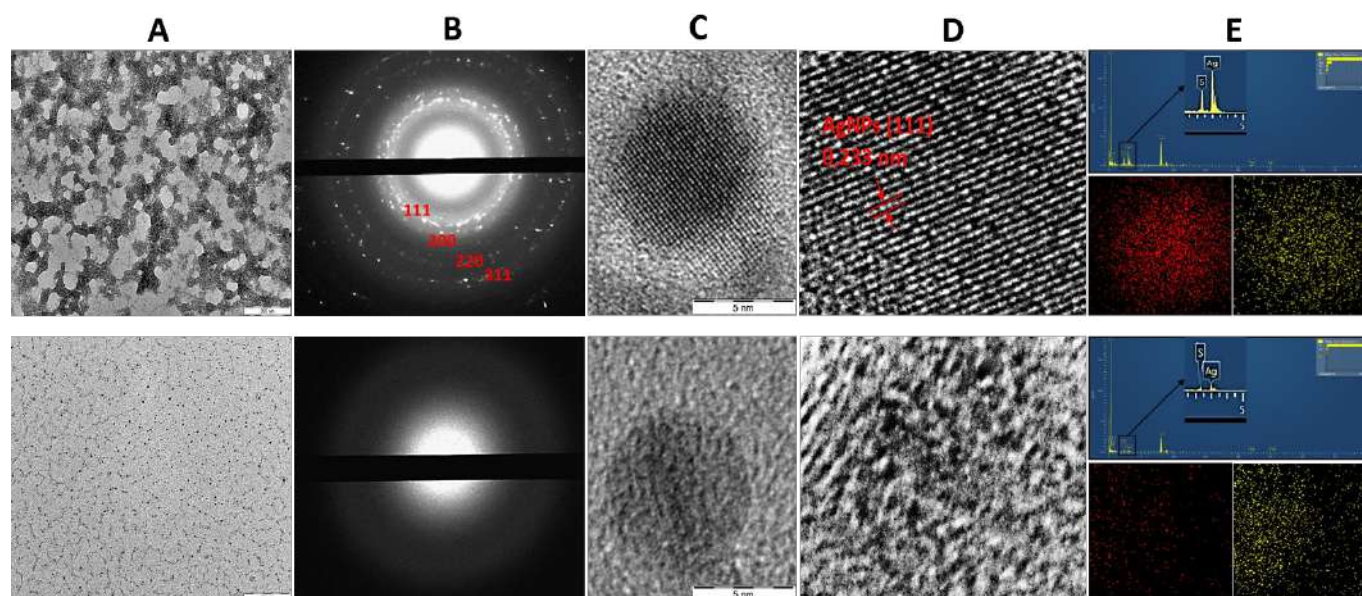


Fig. 3 A – TEM, B – SAED, C, D – HRTEM, E – EDX mapping analysis (red and yellow colour – silver and sulphur atoms respectively) images for CYS-AgNO₂ (Top) and NAC-AgNO₂ (Bottom) systems.

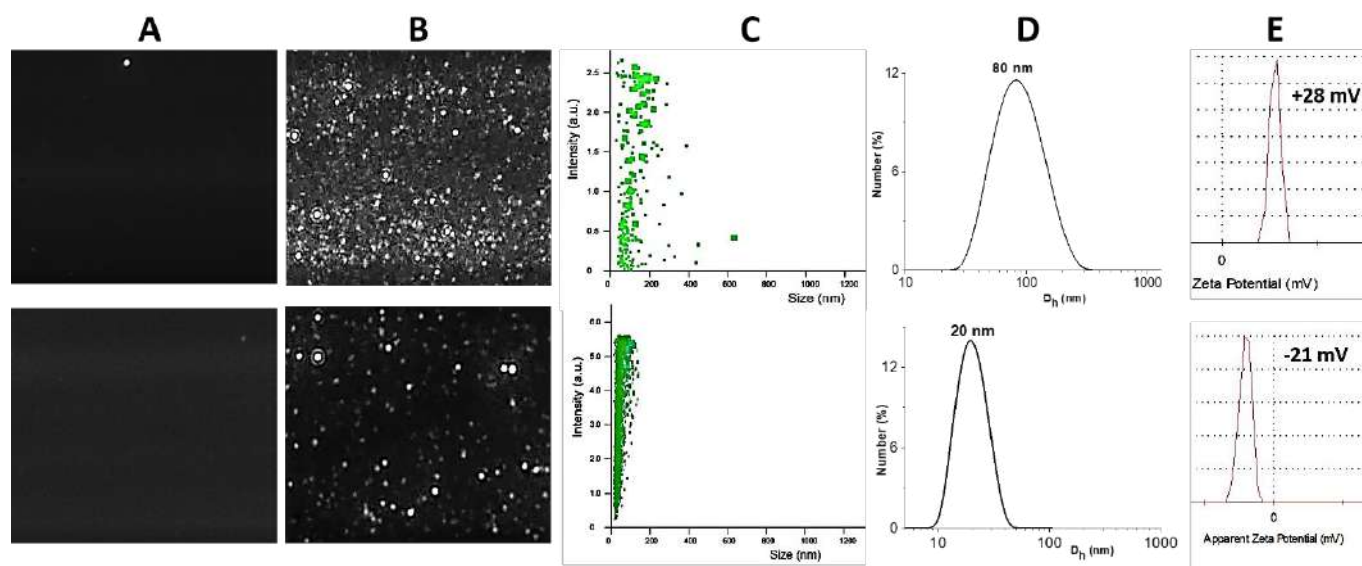


Fig. 4 A, B – NTA instant photos of pure water and SS systems respectively, C – particles size distribution by NTA, D - particles size distribution by DLS, E – zeta-potential measurements for CYS-AgNO₂ (Top) and NAC-AgNO₂ (Bottom) systems.

case. pH of resulted samples is 2.60 – 4.10 in dependence of chemical nature of amino acid and silver salt,²¹ herewith, amino-groups are fully protonated and carboxyl ones partly. pH of initial solutions of amino acids is 5.20-5.40. Thus, the addition of the silver salt to amino acid solution leads to the medium acidification.

FTIR-spectra of initial amino acids change after adding of silver salts (Fig. S8). The same peculiarity for both CYS-AgX and NAC-AgX systems is the disappearance of the $\nu(\text{SH})$ at 2552 cm^{-1} that points to interaction of silver ions with thiol-groups of amino acids.

Summing up of the current data one can propose the following mechanism of the self-assembly (Fig. 5): silver ions interact primarily

with thiol-groups of amino acids that is in a good agreement with Pearson's HSAB (hard and soft (Lewis) acids and bases) theory, meanwhile two parallel reactions may occur – the formation of so-called CYS(NAC)/Ag⁺ complexes and the reduction of Ag⁺ to zero valent state. The presence of Ag⁰ in the systems is beyond doubt. It is known, CYS possesses a middle reduction properties^{43,44} and 15-times higher reduction ability to silver ions compared to hydrazine hydrate.⁴⁵ Herewith, L-cysteine is a stronger reducing agent than N-acetyl-L-cysteine.⁴⁶ That's why crystalline phase of AgNPs occurs only in the presence of CYS, whereas the non-crystalline phase of silver clusters takes place for NAC. The other and more difficult question is

dealt with peculiarities of CYS(NAC)/Ag⁺ complexes formation and their structure. According to our previous,^{21,22,25} present data and literature,⁴⁷⁻⁵⁰ we can propose that CYS/Ag⁺ and NAC/Ag⁺ complexes have the similar structure (Fig. 5, blue chains). The interaction of stabilized AgNPs or AgNCs with these complexes, seemed, proceeds via formation of hydrogen bonds between charged amino- and carboxyl groups in the case of CYS systems (Fig. 5, a) or partly protonated carboxyl groups for NAC ones (Fig. 5, b) and it leads to the formation of final particles. Furthermore, complexes interact with each other via hydrogen bonding and form sandwich-like shell. Thus, particles are constructed from the core of AgNPs or AgNCs and shell of CYS/Ag⁺ or NAC/Ag⁺ complexes. Amino- and carboxyl groups are located on the surface of particles and responsible for their solubility and colloidal stability of systems. Meanwhile, the smaller hydrodynamic parameters of particles in NAC systems are due to the fact that most of NAC/Ag⁺ complexes interact with silver clusters and form the particle core, these data are consistent with HRTEM and EDX mapping analysis. In confirmation of such structure of particles for NAC systems is the fact that LSPR occurs also on the surface of small individual silver clusters⁵¹⁻⁵³ but in our case AgNCs link into a single particle and plasmons are seemed quench each other inside of this particle. So, one can expect that the difference in the structural parameters of particles in CYS and NAC systems must significantly affect to it final bioactive properties.

Bioactive properties of CYS-AgNPs and NAC-AgNCs systems

In accordance with the literature, there are a literally several articles related to methods of the synthesis of silver nanoparticles and silver clusters using sulfur-containing amino acids, as well as the study of bioactive properties of obtained compositions (Table 2). All of these synthetic techniques use toxic reducing agents⁵⁴⁻⁵⁸ or additional external exposures,⁵⁹ the antibacterial effect has either not been studied at all, or it is 1-2 orders of magnitude lower compared to studied samples in the present work. Furthermore, investigated systems are not inferior in antibacterial activity to other known silver-based systems.⁶⁰ Concerning systems under study, one can see their activity to gram-negative bacteria is more pronounced than on gram-positive ones (Table 2, Table S1, Fig. S9,1,2). This phenomenon can be explained by existing difference in the thickness of the cell wall in gram-positive (30 nm) and gram-negative (3-4 nm) bacteria.⁶¹ MIC of CYS systems reduced at moving from SS-1 to SS-6 system and further to NAC systems (SS-7 - SS-10) for gram positive bacteria, but its values were practically the same for gram negative ones. The total bioactive effect against all bacteria is twice as high for systems based on NAC. The solutions of initial amino acids showed no activity at concentrations 2 orders of magnitude higher than MIC of SS-1 - SS-10.

It is known, silver ions are more harmful to the various normal human cells than silver nanoparticles.⁶² The other problem is a high reactivity of Ag⁺ to different anionic compounds of blood plasma that leads to precipitation. Reducing the toxicity of silver-based systems is a key task in the development of new drugs for antibacterial

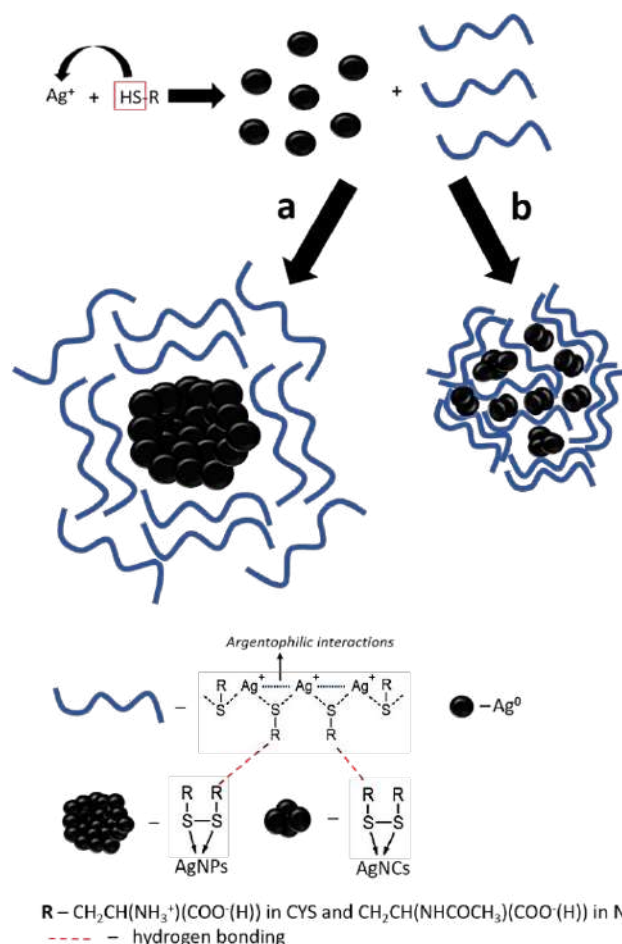


Fig. 5 The proposed mechanism of core-shell like structure particles formation.

Table 2 The synthetic protocol and antibacterial activity (MIC) of SS-1 – SS-10 samples and other related systems to planktonic bacteria.

Sample	Reducing/stabilizing agent	MIC, μM gram-positive/negative bacteria	Ref.
SS-1	CYS/CYS	1500/23,45	Our work
SS-2	CYS/CYS	750/23,45	Our work
SS-3	CYS/CYS	562,5/23,45	Our work
SS-4	CYS/CYS	234,38/23,45	Our work
SS-5	CYS/CYS	281,25/93,75	Our work
SS-6	CYS/CYS	140,63/46,9	Our work
SS-7	NAC/NAC	46,9/11,7	Our work
SS-8	NAC/NAC	93,75/23,45	Our work
SS-9	NAC/NAC	93,75/23,45	Our work
SS-10	NAC/NAC	93,75/23,45	Our work
Ag _n (NALC) _m	NaBH ₄ /NAC	3700/6400	54
nano-Ag	TBAB/CYS	-/93	55
CYS capped AgNPs	NaBH ₄ /CYS	-/-	56
L-CYS-AgNPs	NaBH ₄ /CYS	-/-	57
CYS capped AgNPs	NaBH ₄ /CYS	-/-	58
CYS-AgNPs	UV/CYS	-/-	59

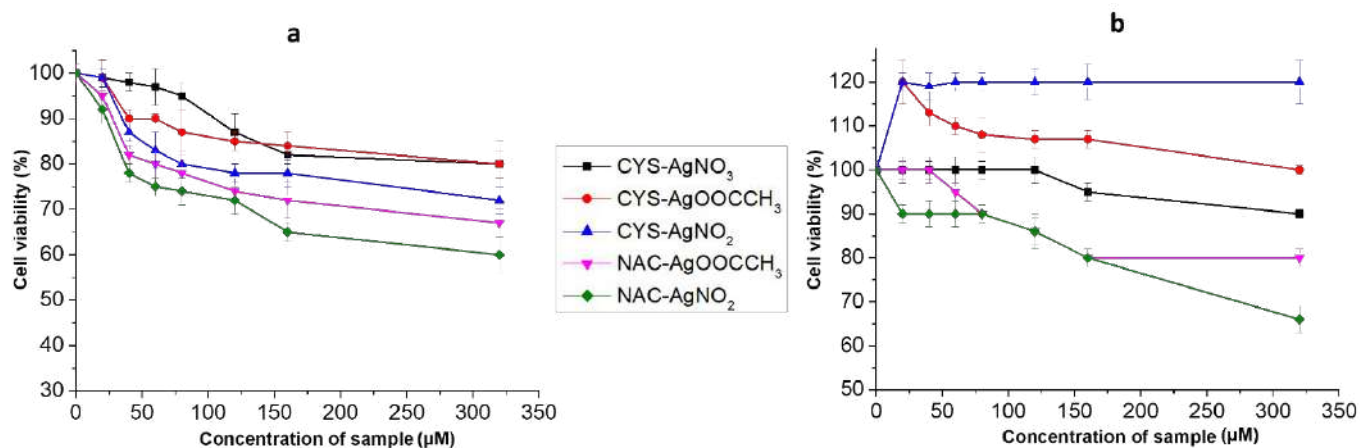


Fig. 6 Cytotoxicity (MTT-test) of CYS-AgNPs and NAC-AgNCs systems to the Wi-38 fibroblast cells (a) and macrophages (b). Wi-38 and macrophage cells incubation with systems is 48 h.

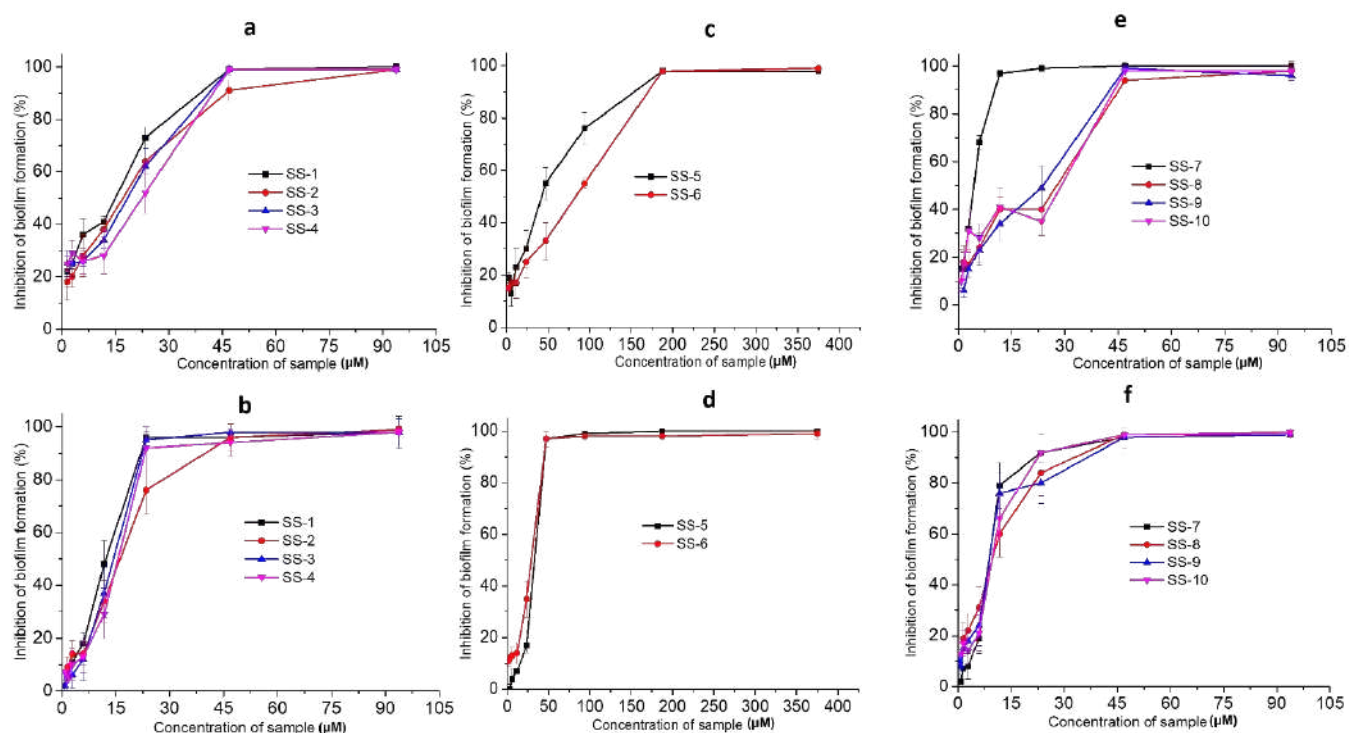


Fig. 7 Antibiofilm activity of SS-1 – SS-10 samples against *P. aeruginosa* (Top) and *A. baumannii* (Bottom): a,b,c,d – CYS-AgNPs and e,f - NAC-AgNCs systems.

therapy. All samples did not cause the lysis of erythrocytes (Table S2). Systems showed low cytotoxicity to fibroblasts and macrophages, its values didn't exceed IC_{50} . The NAC systems were a little more toxic than CYS. Interestingly, some of CYS systems promote macrophages proliferation even at high concentration of the sample. This effect can be connected with the amino acids influence.

Since SS-1 – SS-10 systems showed the highest activity in relation to gram-negative bacteria, studies of their antibiotic film properties were carried out on appropriate bacterial films (Fig. 7). Furthermore, *P. aeruginosa* and *A. baumannii* are the most prominent at forming biofilms amongst the tested in this work and other known bacteria. The activity of samples grows in a row: CYS-AgNO₂ (SS-5, SS-6) < CYS-AgNO₃ and CYS-AgOOCCH₃ (SS-1 – SS-4) < NAC-AgNO₂ (SS-9, SS-10) <

NAC-AgOOCCH₃ (SS-7, SS-8). In all cases NAC systems suppressed the formation of biofilms twice as much as CYS ones for both line of bacterial strains. Herewith, NAC-AgOOCCH₃ (SS-7) turned out to be the most active among all samples and inhibited the biofilms formation at 1×MIC whereas other samples made it from 2×MIC to 4×MIC. It should be noted the SS-7 had a quite low cytotoxicity to normal cells even at concentrations an order of magnitude higher than MIC. The lower toxicity of NAC-AgOOCCH₃ compared to NAC-AgNO₂ can be connected with the more toxic effect of nitrite ions opposed to acetate ones.

According to the proposed structure of nanoparticles (Fig. 5) their surface has positive and negative charge values in CYS-AgX and NAC-AgX systems respectively in the initial solutions (pH<7). But at

conditions of the experiment which corresponds to physiological (pH 7.2–7.4) the equilibrium of the protolytic dissociation shifts towards the formation of $-NH_2$ groups in CYS ($-NH-COCH_3$ in NAC) and COO^- in both systems. Particles surface is charged negatively. The bacterial membrane has a negative charge in the range of -10 to -50 mV of zeta-potential values in dependence of the type of bacteria.⁶³ Thus, the probability of direct binding of nanoparticles to the bacterial membrane surface is unlikely. Although, there are several works where negatively charged AgNPs showed the strong antibacterial effect.^{63,64} We reckon that at $pH > 7$ nanoparticle shell, consisting of CYS/Ag⁺ or NAC/Ag⁺ complexes, start destroying due to the repulsion of fully deprotonated negatively charged carboxylic groups that leads to breaking of hydrogen bondings (Fig. 5). Silver-sulfur bonds in complexes are seemed also broken down. As a result, there are a release of silver ions and cores of AgNPs or AgNCs. These species react with thiol-containing proteins of bacterial membrane because of the high affinity of silver to sulphur or cause ROS thereby disrupting its functions and leading to the death of bacteria. Herewith AgNCs are more active than AgNPs due to their smaller size and greater mobility. Moreover, according to Ostwald–Freundlich equation, smaller silver particles are more susceptible to the release of Ag⁺ ions owing to their greater surface area. If the initial nanoparticles are able to penetrate the membrane of bacteria, then NAC systems will make it easier due to the smaller hydrodynamic particle sizes. Concerning inhibitory ability of systems to biofilms formation the additional and important influence may also have amino acids since it is known, L-cysteine and more N-acetyl-L-cysteine possess antibiofilm activity in the concentration range of 0,01 – 0,5 M.^{65,66} This effect is dealt with the possibility of CYS and NAC thiol-groups partaking in the thiol-disulfide exchange and thus destructing of $-S-S-$ bonds which are responsible for stabilizing the hydrophobic surface of biofilms.⁶⁷ Indeed, after destruction of CYS/Ag⁺ and NAC/Ag⁺ complexes and releasing of Ag⁺, free CYS and NAC moieties form with protonated thiol-group (pK_a (SH) = 9.52). The elucidation of the mechanism of interaction of investigated systems with bacteria and biofilms **as well as carrying out *in vivo* experiments** is the subject of further research.

Conclusions

In this work **nanosilver-based sols and hydrogels with core-shell like structure of particles** were prepared using the L-cysteine and N-acetyl-L-cysteine as bio-reducing agents at ambient conditions without any additional components or other exposures. The chemical nature of the amino acid dramatically influenced the final microstructure of resulting materials that is obtaining of silver nanoparticles and silver clusters in the case of CYS and NAC respectively. This peculiarity defined stronger antibacterial and antibiofilm properties of NAC-based systems than CYS ones. Therefore, the novel CYS-AgNPs and NAC-AgNCs systems obtained via the **simple “green” chemistry technique** can be potentially used as alternative materials against various bacterial infections mediated by biofilms formation.

Author Contributions

Results were interpreted and the manuscript was written by D.V.V. D.V.V. supervised all the structural experiments. The synthesis and physicochemical analysis were carried out by D.V.A. and D.V.V. Microscopic studies were performed by A.A.E. and A.A.L. MTT-test data were received by A.R.M. Hemolysis, antibacterial and biofilms formation assays were performed by E.V.V. and M.S.S. under supervision of O.V.S. All authors have given approval to the final version of the manuscript and declare no competing financial interest.

Conflicts of interest

There are no conflicts to declare.

Acknowledgements

This work was carried out with the financial support of Russian Science Foundation № 21-73-00134 on the equipment of the Shared Facility Centre of Tver State University.

Notes and references

- M. Assefa, A. Amare, *Infect. Drug Resist.*, 2022, **15**, 5061–5068.
- J.L. Del Pozo, *Expert Rev. Anti-Infect. Ther.*, 2018, **16**, 51–65.
- C.A. Arias, B.E. Murray, *N. Engl. J. Med.*, 2015, **372**, 1168–1170.
- D. Sharma, L. Misba, A.U. Khan, *Antimicrob. Resist. Infect. Control*, 2019, **8**, 76–86.
- A. Ghosh, N. Jayaraman, D. Chatterji, *ACS Omega*, 2020, **5**, 3108–3115.
- F. Cui, T. Li, D. Wang, S. Yi, J. Li, X. Li, *J. Hazard. Mater.*, 2022, **431**, 1285–1297.
- L.D. Blackman, Y. Qu, P. Cass, K.E.S. Locock, *Chem. Soc. Rev.*, 2021, **50**, 1587–1616.
- S. Qayyum, A.U. Khan, *Med. Chem. Comm.*, **7**, 1479–1498.
- K. McNamara, S.A.M. Tofail, *Adv. Phys-X*, 2017, **2**, 54–88.
- M. Jiao, P. Zhang, J. Meng, Y. Li, C. Liu, X. Luo, M. Gao, *Biomater. Sci.*, 2018, **6**, 726–745.
- A.-C. Burdusel, O. Gherasim, A.M. Grumezescu, L. Mogoanta, A. Ficai, E. Andronescu, *Nanomaterials*, 2018, **8**, 681–705.
- A. Roy, O. Bulut, S. Some, A.K. Mandal, M.D. Yilmaz, *RSC Adv.*, 2019, **9**, 2673–2702.
- L. Xu, Y.-Y. Wang, J. Huang, C.-Y. Chen, Z.-X. Wang, H. Xie, *Theranostics*, 2020, **10**, 8996–9031.
- K.R.B. Singh, V. Nayak, J. Singh, A.K. Singh, R.P. Singh, *RSC Adv.*, 2021, **11**, 24722–24746.
- A. Nicolae-Maranciuc, D. Chicea, L.M. Chicea, *Int. J. Mol. Sci.*, 2022, **23**, 5778–5808.
- S.H. Lee, B.-H. Jun, *Int. J. Mol. Sci.*, 2019, **20**, 865–888.
- L.E. Valenti, C.E. Giacomelli, *J. Nanopart. Res.*, 2017, **19**, 156–165.
- S. Shankar, J.-W. Rhim, *Carbohydr. Polym.*, 2015, **130**, 353–363.
- R.A. Matos, L.C. Courrol, *Amino Acids*, 2017, **49**, 379–388.
- D.I. Saragiha, D.C.V. Arifin, B. Rusdiarso, S. Suyanta, S.J. Santos, *Key Eng. Mat.*, 2019, **840**, 360–367.
- D.V. Vishnevskii, A.R. Mekhtiev, T.V. Perevozova, A.I. Ivanova, D.V. Averkin, S.D. Khizhnyak, P.M. Pakhomov, *Soft Matter*, 2022, **18**, 3031–3040.
- D.V. Vishnevskii, A.R. Mekhtiev, T.V. Perevozova, D.V. Averkin, A.I.

- Ivanova, S.D. Khizhnyak and P.M. Pakhomov, *Soft Matter*, 2020, **16**, 9669-9673.
- 23 D.V. Vishnevetskii, A.I. Ivanova, S.D. Khizhnyak, P.M. Pakhomov, *Fibre Chemistry*, 2021, **53**, 5-10.
- 24 D.I. Belenkii, D.V. Averkin, D.V. Vishnevetskii, S.D. Khizhnyak, P.M. Pakhomov, *Measurement Techniques*, 2021, **64**, 328-332.
- 25 D.V. Vishnevetskii, D.V. Averkin, A.A. Efimov, A.A. Lizunova, A.I. Ivanova, P.M. Pakhomov, E. Ruehl, *Soft Matter*, 2021, **17**, 10416-10420.
- 26 K. Zheng, X. Yuan, N. Goswami, O. Zhang, J. Xie, *RSC Adv.*, 2014, **4**, 60581-60596.
- 27 Y.-P. Xie, Y.-L. Shen, G.-X. Duan, J. Han, L.-P. Zhang, X. Lu, *Mater. Chem. Front.*, 2020, **4**, 2205-2222.
- 28 Y. Xia, D. J. Campbell, *J. Chem. Educ.* 2007, **84**, 91-96.
- 29 J.C. Fuentes, J. Rivas, M.A. Lopez-Quintela, *Encycl. Nanotechnol*, 2011, 1-15.
- 30 K.V. Mrudula, T.U.B. Rao, T. Pradeep, *J. Mater. Chem.*, 2009, **19**, 4335-4342.
- 31 X. Yuan, M.I. Setyawati, D.T. Leong, J. Xie, *Nano Res.*, 2013, **7**, 301-307.
- 32 X.-R. Song, N. Goswami, H.-H. Yang, J. Xie, *Analyst*, 2016, **141**, 3126-3140.
- 33 C.P. Joshi, M.S. Bootharaju, M.J. Alhilaly, O.M. Bakr, *J. Am. Chem. Soc.*, 2015, **137**, 11578-11581.
- 34 A.M. Perez-Marino, M.C. Blanco, D. Buceta, M.A. Lopez-Quintela, *J. Chem. Educ.*, 2019, **96**, 558-564.
- 35 X.L. Guével, C. Spies, N. Daum, G. Jung, M. Schneider, *Nano Res.*, 2012, **5**, 379-387.
- 36 L. Dhanalakshmi, T. Udayabhaskararao, T. Pradeep, *Chem. Commun.*, 2012, **48**, 859-861.
- 37 E. Khatun, A. Ghosh, D. Ghosh, P. Chakraborty, A. Nag, B. Mondal, S. Chennu, T. Pradeep, *Nanoscale*, 2017, **9**, 8240-8248.
- 38 L.G. AbdulHalim, N. Kothalawala, L. Sinatra, A. Dass, O.M. Bakr, *J. Am. Chem. Soc.*, 2014, **136**, 15865-15868.
- 39 R. Jin, C. Zeng, M. Zhou, Y. Chen, *Chem. Rev.*, 2016, **116**, 10346-10413.
- 40 I. Chakraborty, T. Pradeep, *Chem. Rev.*, 2017, **117**, 8208-8271.
- 41 J. Yan, B.K. Teo, N. Zheng, *Acc. Chem. Res.*, 2018, **51**, 3084-3093.
- 42 T.V. Potapenkova, D.V. Vishnevetskii, A.I. Ivanova, S.D. Khizhnyak, P.M. Pakhomov, *Russ. Chem. Bull.*, 2022, **71**, 2123-2129.
- 43 B. Sharma, M.K. Rabinal, *J. Alloys Compd.*, 2015, **649**, 11-18.
- 44 Z. Chen, Y. Shen, A. Xie, J. Zhu, Z. Wu, F. Huang, *Cryst. Growth Des.*, 2009, **9**, 1327-1333.
- 45 J.I. Hussain, S. Kumar, A.A. Hashmi, Z. Khan, *Adv. Matt. Lett.*, 2011, **2**, 188-194.
- 46 A.S. Prakasha Gowda, A. Schaefer, T. Schuck, *Cell and Gene Therapy Insights*, 2020, **6**, 303-323.
- 47 R. A. Bell, *Environ. Toxicol. Chem.*, 1999, **18**, 9-22.
- 48 J.-S. Shen, D.-H. Li, M.-B. Chang, J. Zhou, H. Zhang, Y.-B. Jiang, *Langmuir*, 2011, **27**, 481-486.
- 49 R. Randazzo, A. D. Mauro, A. D'Urso, G. C. Messina, G. Compagnini, V. Villari, N. Micali, R. Purrello and M. E. Fragala, *J. Phys. Chem. B*, 2015, **119**, 4898-4904.
- 50 B. O. Leung, F. Jalilehvand, V. Mah, M. Parvez, Q. Wu, *Inorg. Chem.*, 2013, **52**, 4593-4602.
- 51 C. Zhang, K. Wang, C. Li, Y. Liu, H. Fu, F. Pan, D. Cui, *J. Mat. Chem. B*, 2014, **2**, 6931-6938.
- 52 D. Li, B. Kumari, J.M. Makabenta, B. Tao, K. Qian, X. Mei, V.M. Rotello, *J. Mat. Chem. B*, 2020, **8**, 9466-9480.
- 53 Z. Ye, H. Zhu, S. Zhang, J. Li, J. Wang, E. Wang, *J. Mat. Chem. B*, 2021, **9**, 307-313.
- 54 K. Wang, Y. Wu, H. Li, M. Li, D. Zhang, H. Feng, H. Fan, *RSC Adv.*, 2014, **4**, 5130-5135.
- 55 J.H. Priester, A. Singhal, B. Wu, G.D. Stucky, P.A. Holden, *Analyst*, 2014, **139**, 954-963.
- 56 B.R. Khalkho, R. Kurrey, M.K. Deb, K. Shrivastava, S.S. Thakur, S. Pervez, V.K. Jain, *Helion*, 2020, **6**, e03423.
- 57 S. Panhwar, S.S. Hassan, R.B. Mahar, A. Canlier, M. Arain, *J. Inorg. Organomet. Polym. Mater.*, 2018, **28**, 863-870.
- 58 S. Mandal, A. Gole, N.L. Rajesh, V. Ganvir, M. Sastry, *Langmuir*, 2001, **17**, 6262-6268.
- 59 H. Liu, Y. Ye, J. Chen, D. Lin, Z. Jiang, Z. Liu, B. Sun, L. Yang, J. Liu, *Chem. Eur. J.*, 2012, **18**, 8037-8041.
- 60 S.A. Ahmad, S.S. Das, A. Khatoun, M.T. Ansari, M. Afzal, M.S. Hasnain, A.K. Nayak, *Mater. Sci. Energy Technol.*, 2020, **3**, 756-769.
- 61 T. Chatterjee, B.K. Chatterjee, D. Majumdar, P. Chakrabarti, *Biochim. Biophys. Acta.*, 2015, **1850**, 299-306.
- 62 M. Akter, Md.T. Sikder, Md.M. Rahman, A.K.M. Ullah, K.F.B. Hossain, S. Banik, T. Hosokawa, T. Saito, M. Kurasaki, *J. Adv. Res.*, 2018, **9**, 1-16.
- 63 A.P.V. Ferreyra Maillard, J.C. Espeche, P. Maturana, A.C. Cutro, A. Hollmann, *BBA Biomembranes*, 2021, **1863**, 183597.
- 64 L. Salvioni, E. Galbiati, V. Collico, G. Alessio, S. Avvakumova, F. Corsi, P. Tortora, D. Prospero, M. Colombo, *Int. J. Nanomedicine*, 2017, **12**, 2517-2530.
- 65 G. Zara, M.B. Zeidan, F. Fancello, M.L. Sanna, I. Mannazzu, M. Budroni, S. Zara, *Appl. Microbiol. Biotechnol.*, 2019, **103**, 7675-7685.
- 66 F. Blasi, C. Page, G.M. Rossolini, L. Pallecchi, M.G. Matera, P. Rogliani, M. Cazzola, *Respiratory Medicine*, 2016, **117**, 190-197.
- 67 B. Pedre, U. Barayeu, D. Ezerina, T.P. Dick, *Pharmacology and Therapeutics*, 2021, **228**, 107916.

L-cysteine and N-acetyl-L-cysteine mediated synthesis of nanosilver-based sols and hydrogels with antibacterial and antibiofilm properties

Dmitry V. Vishnevetskii,^{a*} Dmitry V. Averkin,^{a,b} Alexey A. Efimov,^c Anna A. Lizunova,^c Olga V. Shamova,^d Elizaveta V. Vladimirova,^d Maria S. Sukhareva^d and Arif R. Mekhtiev^e

^a Department of Physical Chemistry, Tver State University, Tver 170100, Russia;

^b Russian metrological institute of technical physics and radio engineering, Moscow 141570, Russia

^c Moscow Institute of Physics and Technology, National Research University, Dolgoprudny 141701, Russia

^d World-Class Research Center “Center for Personalized Medicine”, Institute of Experimental Medicine, St. Petersburg 197376, Russia

^e Institute of Biomedical Chemistry, Moscow 191121, Russia

*Correspondence: rickashet@yandex.ru (D.V.V.).

Contents

Synthesis of CYS-AgNPs and NAC-AgNCs.....	S2
UV analysis.....	S2
TEM, SAED and EDX mapping analysis.....	S3
AFM, SEM, EDX and ICP-MS analysis.....	S5
NTA and DLS.....	S6
FTIR analysis.....	S6
Antibacterial assay.....	S7
Hemolysis assay and MTT-test.....	S9

Synthesis of CYS-AgNPs and NAC-AgNCs

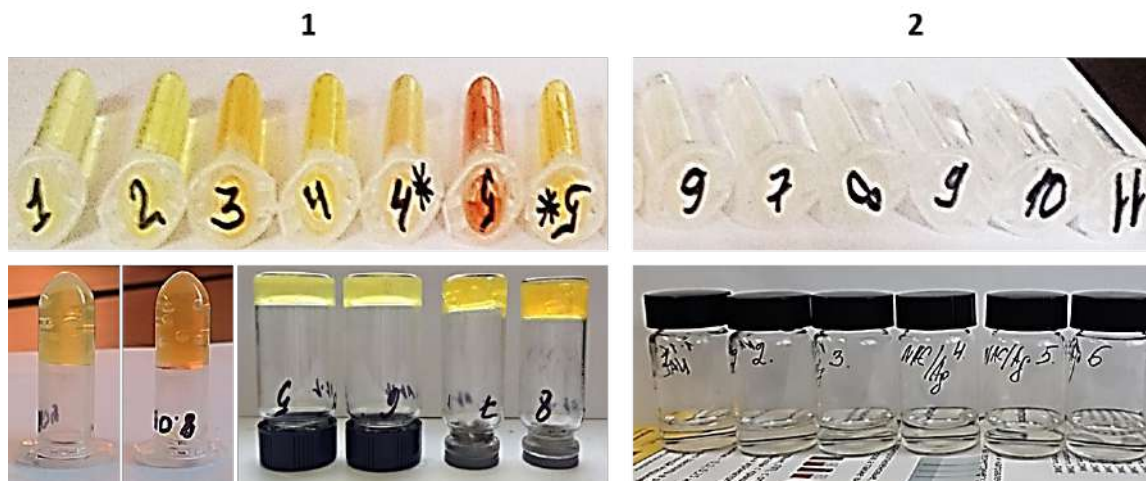


Fig. S1 Systems obtained after 3h at mixing of AgX (X = NO₂⁻, CH₃COO⁻ or NO₃⁻) with CYS (1) and NAC (2) in the concentration range of the dispersed phase from 1 to 20 mM.

UV analysis

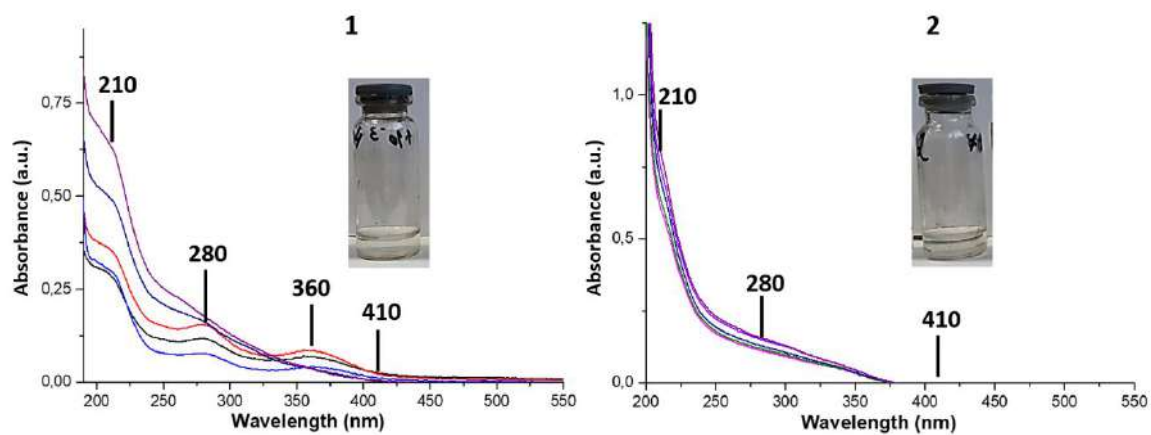


Fig. S2 UV spectra of systems obtained after 3h at mixing of AgX (X = NO₂⁻, CH₃COO⁻ or NO₃⁻) with CYS (1) and NAC (2) at the concentration of the dispersed phase < 1mM. C(CYS) = C(NAC) = 0,3 mM, C(AgX) = 0,15 mM – 0,6 mM.

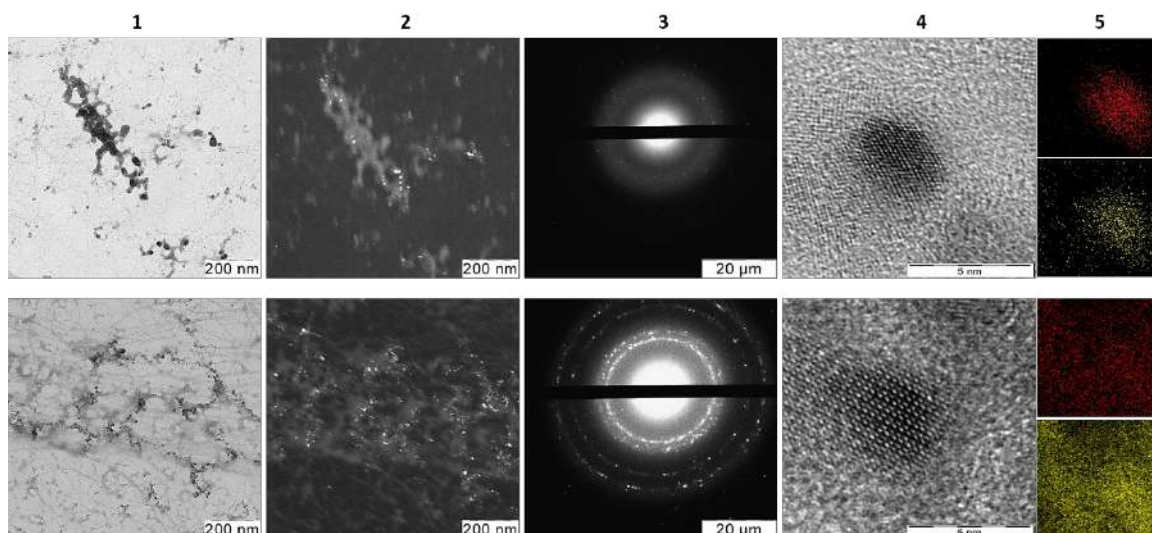
TEM, SAED and EDX mapping analysis

Fig. S3 1 – bright-field TEM, 2 – dark-field TEM, 3 – SAED, 4 – HRTEM, 5 – EDX mapping analysis (red and yellow colour – silver and sulphur atoms respectively) images for CYS-AgNO₃ systems.

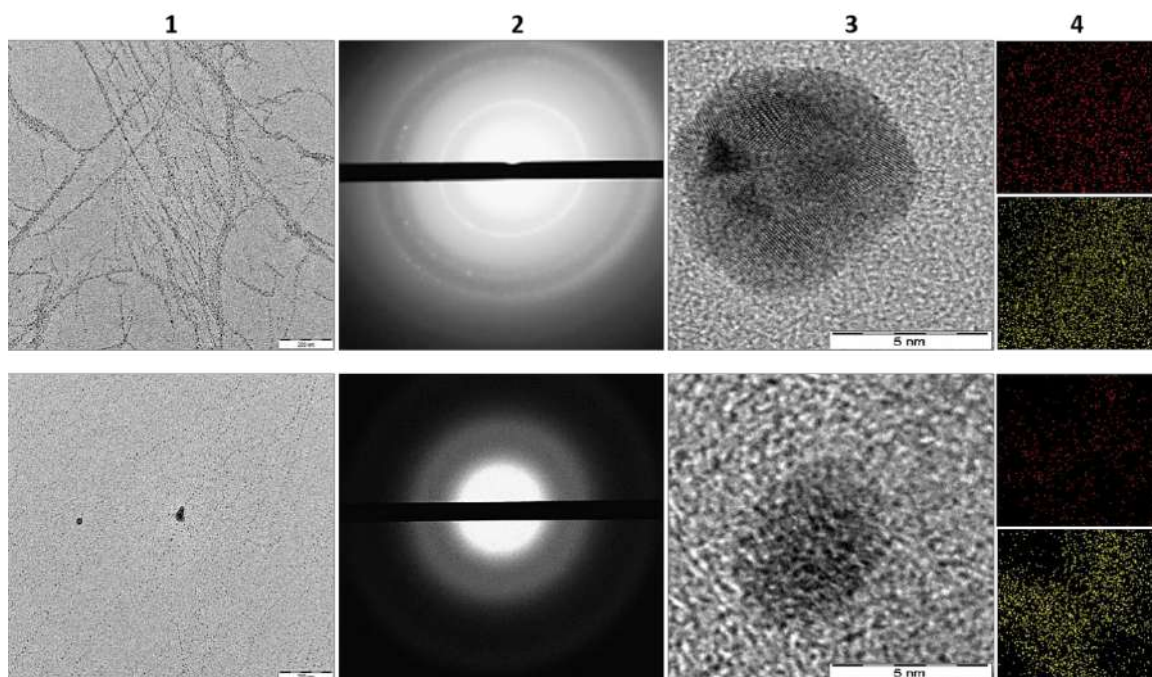


Fig. S4 1 – TEM, 2 – SAED, 3 – HRTEM, 4 – EDX mapping analysis (red and yellow colour – silver and sulphur atoms respectively) images for CYS-AgOOCCH₃ (**Top**) and NAC-AgOOCCH₃ (**Bottom**) systems.

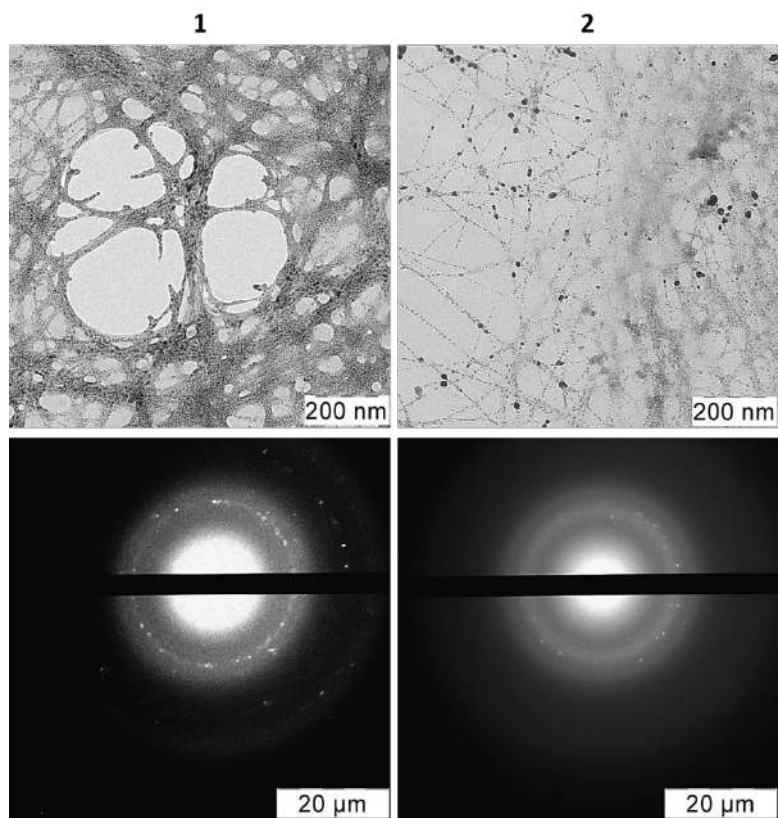


Fig. S5 TEM (**Top**) and SAED (**Bottom**) for CYS-AgNO₃-Na₂SO₄ (**1**) and CYS-AgOOCCH₃-Na₂SO₄ (**2**) systems.

AFM, SEM, EDX and ICP-MS analysis

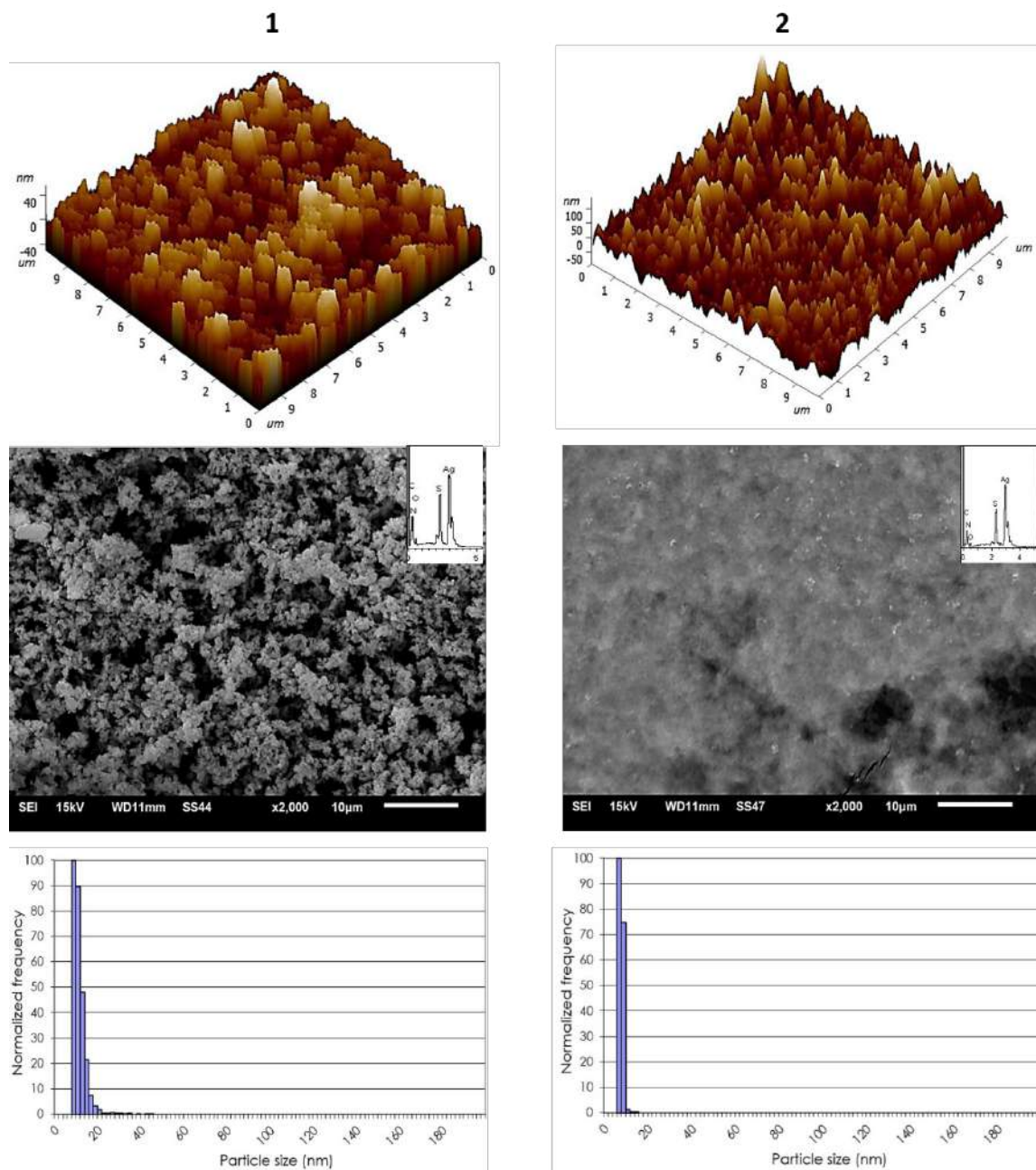


Fig. S6 AFM (Top), SEM (Middle), EDX (Middle, upper right corner) and ICP-MS (Bottom) analysis for CYS-AgX (1) and NAC-AgX (2) systems.

NTA and DLS

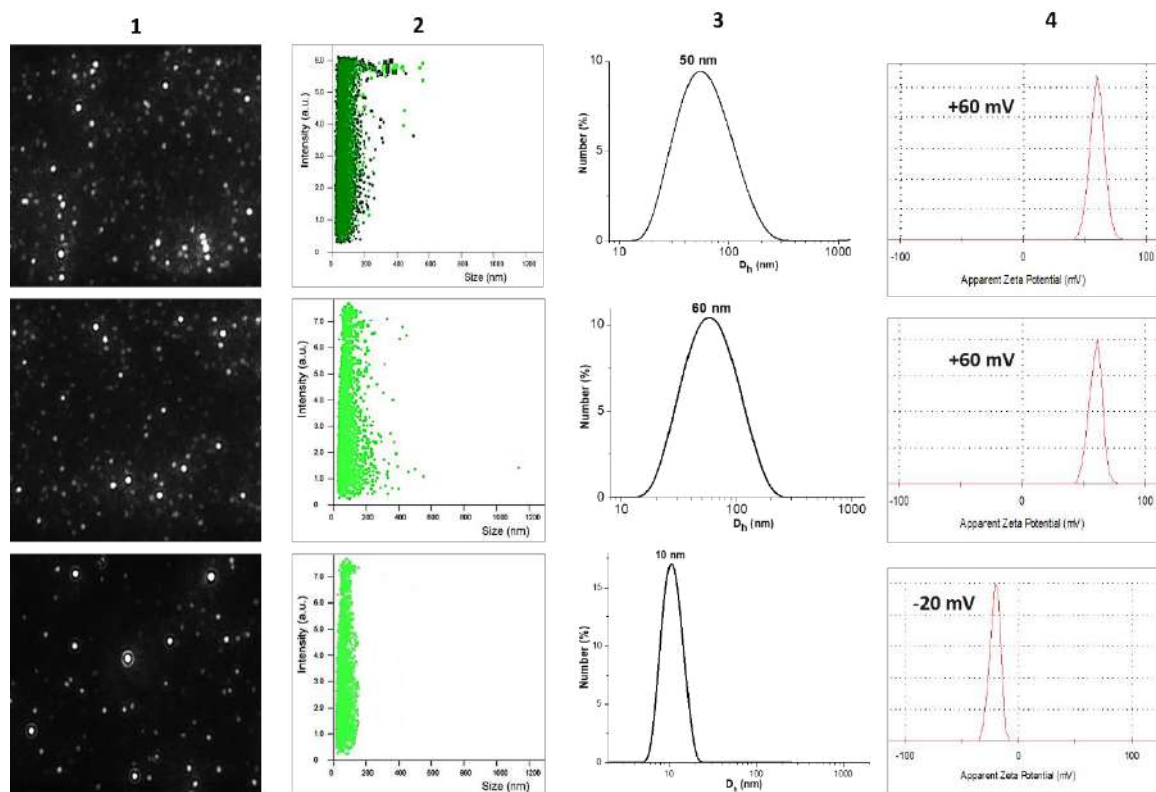


Fig. S7 1 – NTA instant photos, 2 - particles size distribution by NTA, 3 - particles size distribution by DLS, 4 – zeta-potential measurements for CYS-AgNO₃ (**Top**), CYS-AgOOCCH₃ (**Middle**) and NAC-AgOOCCH₃ (**Bottom**).

FTIR analysis

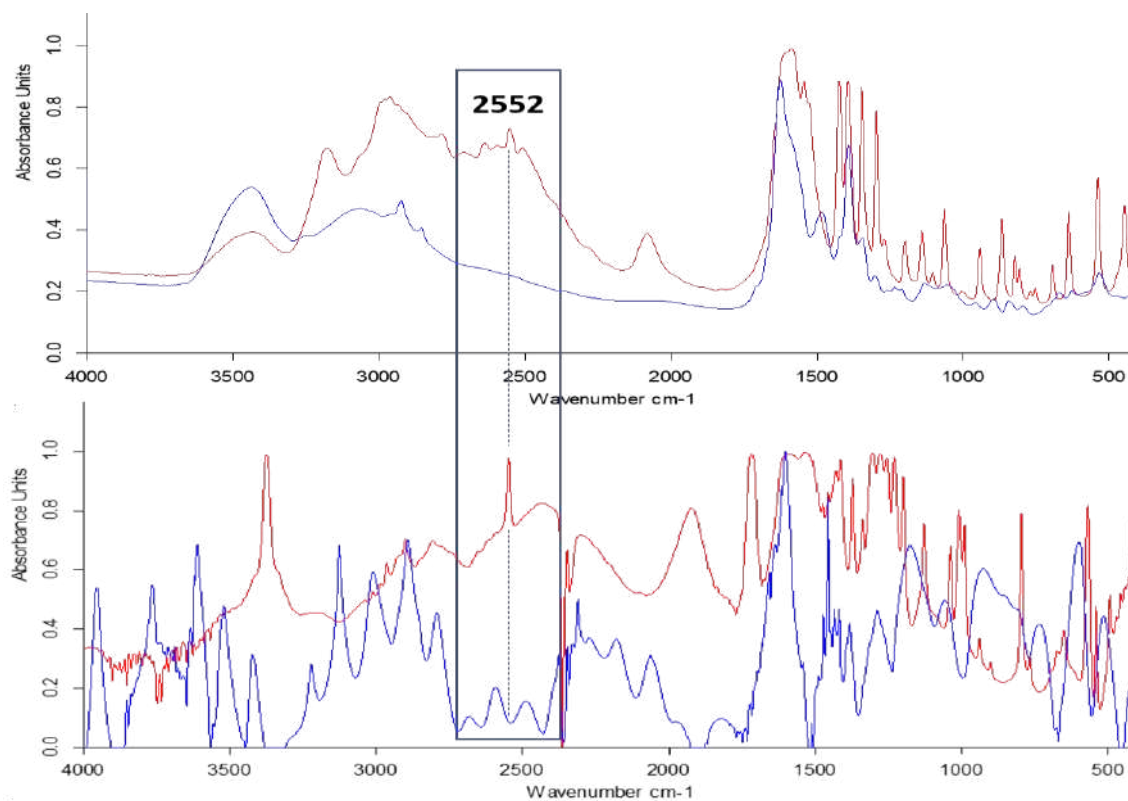


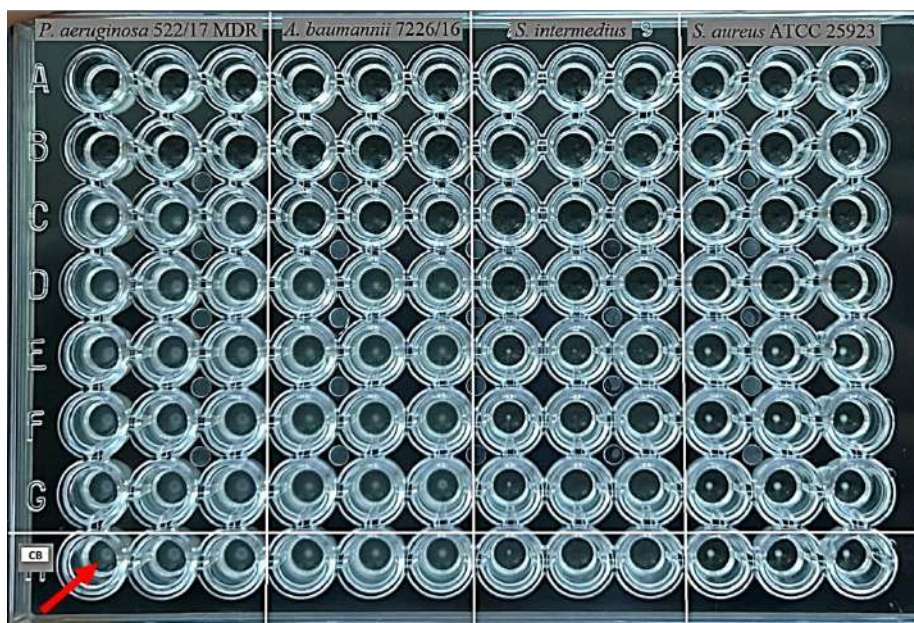
Fig. S8 FTIR spectra of CYS (**Top**, red color), NAC (**Bottom**, red color), CYS-AgX (**Top**, blue color) and NAC-AgX (**Bottom**, blue color).

Antibacterial assay

Table S1 Minimum concentrations of studied substances inhibiting the growth of microorganisms (MIC).

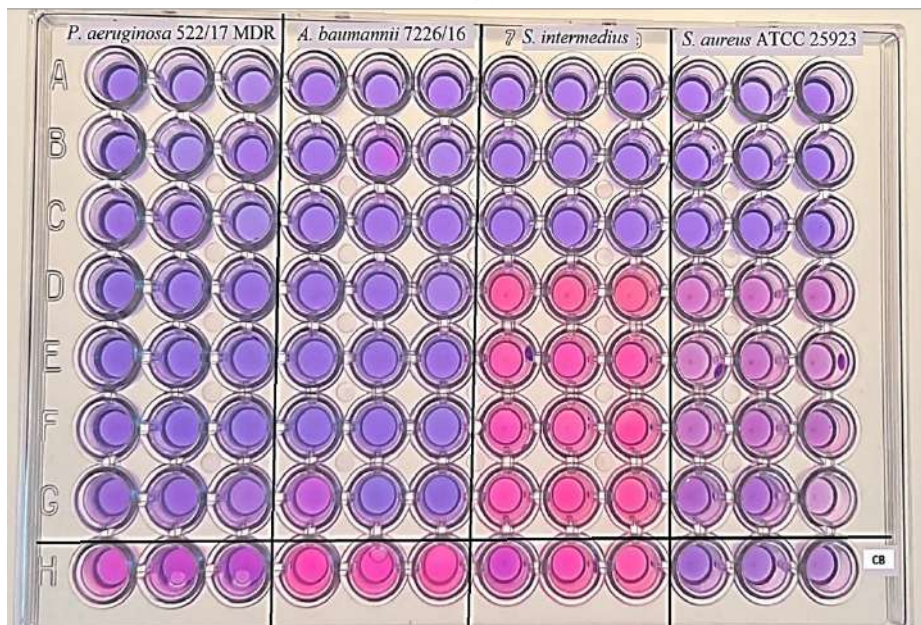
Bacteria/Sample	MIC, μM			
	Gram-negative		Gram-positive	
	<i>P. aeruginosa</i> 522/17 MDR	<i>A. baumannii</i> 7226/16	<i>S. intermedius</i>	<i>S. aureus</i> ATCC 25923
SS-1	23,45	23,45	>1500	>1500
SS-2	23,45	35,18	1500	750
SS-3	23,45	23,45	>1500	562,5
SS-4	35,18	23,45	281,25	234,38
SS-5	93,75	93,75	281,25	375
SS-6	70,33	46,9	140,63	140,63
SS-7	11,7	23,45	46,9	46,9
SS-8	23,45	23,45	93,75	93,75
SS-9	23,45	46,9	187,5	93,75
SS-10	23,45	46,9	93,75	93,75

1



Sample concentration, μM	<i>P. aeruginosa</i> 522/17 MDR						<i>A. baumannii</i> 7226/16						<i>S. intermedius</i>						<i>S. aureus</i> ATCC 25923						Sample concentration, μM						
93,75																															750
46,9																															375
23,4	+	+	+	+	+	+	+	+	+	+	+	+																			187,5
11,7	+	+	+	+	+	+	+	+	+	+	+	+																			93,75
5,85	+	+	+	+	+	+	+	+	+	+	+	+	+	+	+	+	+	+	+	+	+	+	+	+	+	+	+	+	+	+	46,9
2,93	+	+	+	+	+	+	+	+	+	+	+	+	+	+	+	+	+	+	+	+	+	+	+	+	+	+	+	+	+	+	23,4
1,46	+	+	+	+	+	+	+	+	+	+	+	+	+	+	+	+	+	+	+	+	+	+	+	+	+	+	+	+	+	+	11,7
Control of bacteria	+	+	+	+	+	+	+	+	+	+	+	+	+	+	+	+	+	+	+	+	+	+	+	+	+	+	+	+	+	+	Control of bacteria

2

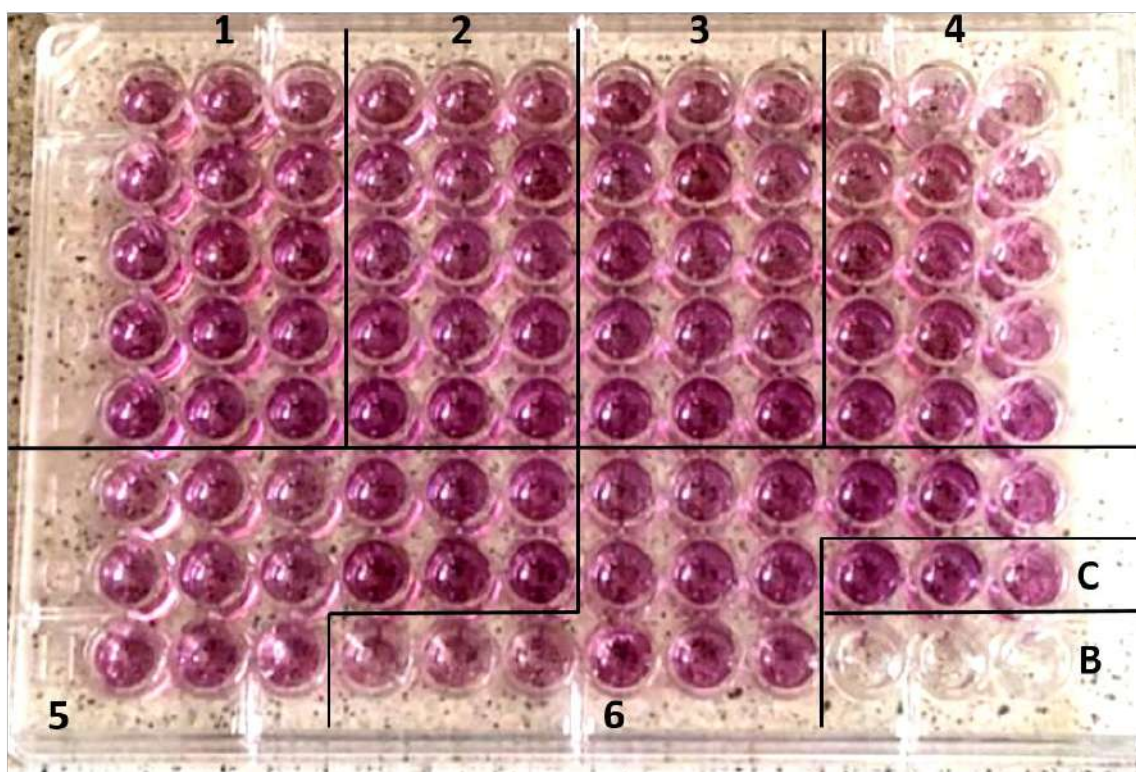


Sample concentration, μM	<i>P. aeruginosa</i> 522/17 MDR			<i>A. baumannii</i> 7226/16			<i>S. intermedius</i>			<i>S. aureus</i> ATCC 25923			Sample concentration, μM
1500													375
750													187,5
375													93,75
187,5							+	+	+	+	+	+	46,9
93,75							+	+	+	+	+	+	23,4
46,9							+	+	+	+	+	+	11,7
23,4				+	+	+	+	+	+	+	+	+	5,85
Control of bacteria	+	+	+	+	+	+	+	+	+	+	+	+	Control of bacteria

Fig. S9 1 – (Top) A photograph of a 96-well plate in which serial double dilutions of sample SS-10 (as an example) were filled from the 1st to the 7th row in 3 parallels. Probes of bacterial growth control – CB (samples that do not contain the sample under study) were placed horizontally in the 8th row. The red arrow marks an example of a visible sediment indicating the growth of a bacterium. **1 – (Bottom)** The schematic image of a 96-well plate, "+" is the visible growth of bacteria by the eye. **2 – (Top)** A photograph of a 96-well plate at determining the MIC of sample SS-10 (as an example) in relation to the studied bacteria. Blue wells – the microorganism is absent or there is no metabolic activity; pink wells – the presence of active metabolism; purple wells - reduced metabolic activity. **2 – (Bottom)** The schematic image of a 96-well plate, "+" is the visible growth of bacteria by the eye.

Hemolysis assay and MTT test**Table S2** Hemolytic activity of studied samples at a concentration of 300 μ M.

Samples	OD ₅₄₀	% of hemolysis	Samples	OD ₅₄₀	% of hemolysis
SS-1	0,072±0,002	0,52	SS-6	0,074±0,003	0,07
SS-2	0,064±0,003	0	SS-7	0,080±0,003	0,48
SS-3	0,064±0,003	0,02	SS-8	0,069±0,006	0
SS-4	0,066±0,005	0,16	SS-9	0,068±0,009	0
SS-5	0,061±0,003	0	SS-10	0,065±0,001	0
«-» control	0,064±0,003	0	«-» control	0,073±0,058	0
«+» control	1,543±0,030	100	«+» control	1,611±0,058	100



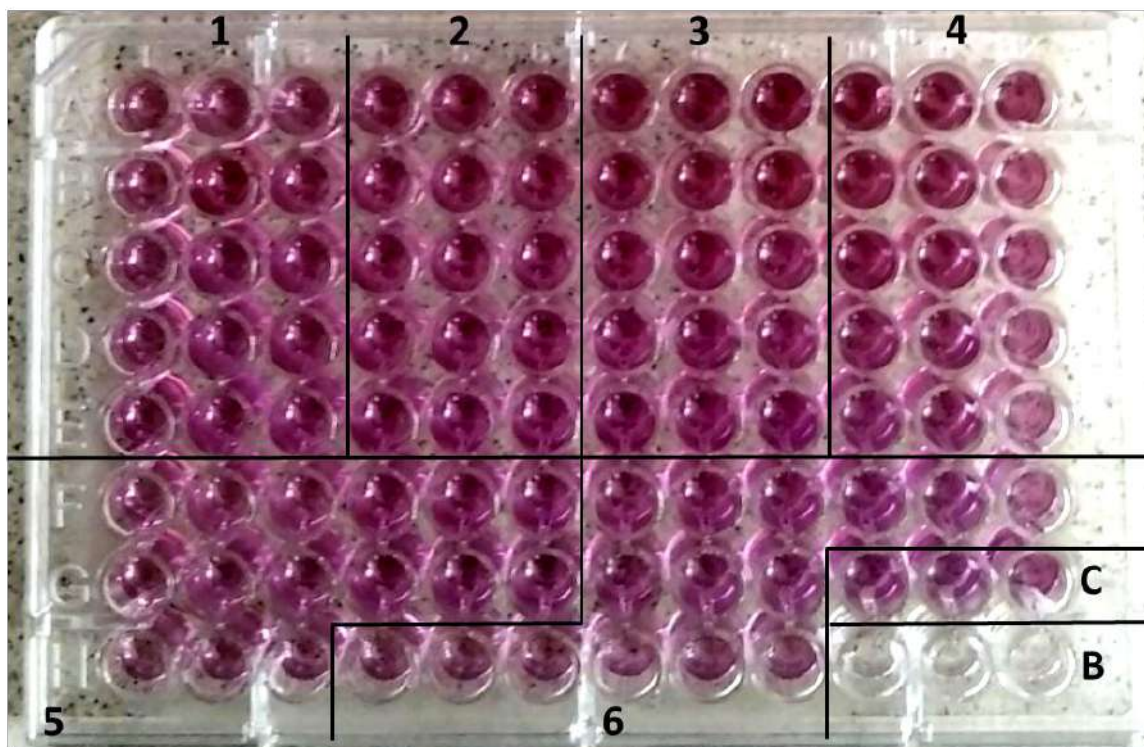


Fig. S9 MTT test of investigated systems to fibroblasts (**Top**) and macrophages (**Bottom**): **1** – CYS-AgNO₃, **2** – CYS-AgOOCCH₃, **3,4** – CYS-AgNO₂, **5** – NAC-AgOOCCH₃, **6** – NAC-AgNO₂. **C** – control (cells without the sample), **B** – blank (empty wells). Cells incubation with systems is 48 h.

Dear Prof. J. Winter,

I am sorry to trouble you, I just wanted to say, that according to referees remarks I marked with green color that I changed in the manuscript. Concerning referee's questions about *in vivo* experiments and additional analysis of particles structure, it is not easy to do them quickly because of gathering summer time, colleagues are preparing different scientific reports and so on. Furthermore, I need to finish my grant report till 15 of May, I just don't have enough time. But anyway, we will carry out these experiments, probably, autumn and describe them in the next manuscript.

Thank you very much!

Sincerely yours,

Dmitry Vishnevetskii.